frontiers in Physics

ORIGINAL RESEARCH
published: 17 July 2020
doi: 10.3389/fphy.2020.00213

Electron Mass Predicted From Substructure Stability in Electrodynamical Model

Stéphane Avner[1]* *and Florence Boillot*[2]

[1] CNRS, Univ Rennes, IGDR-UMR 6290, Rennes, France, [2] COSYS-GRETTIA, Univ Gustave Eiffel, IFSTTAR, Marne-la-Vallée, France

Modern physics has characterized spacetime, the interactions between particles, but not the nature of the particles themselves. Previous models of the electron have not specified its substance nor justified its cohesion. Here we present a relativistic electrodynamical model of the electron at rest, founded on natural interpretations of observables. Essentially intertwined positively and negatively charged subparticles revolve at light velocity in coplanar circular orbits, forming some coherent "*envelope*" and "*nucleus*", possibly responsible for its wavelike and corpuscular behaviors, respectively. We show that the model can provide interpretations of fundamental constants, satisfy the Virial theorem, and exhibit cohesion and stability without invoking Poincaré stresses. Remarkably, the stability condition allows predicting electron mass, regarded as being a manifestation of its total (kinetic and potential) electromagnetic cohesion energy, and muon mass, directly from the substructure. Our study illustrates the possibility of constructing causal and objectively realist models of particles beneath the Compton scale. Finally, wave-corpuscle duality and the relation to quantum mechanics are discussed in the light of our electron model.

Keywords: electron substructure, fundamental constants, electromagnetic mass, wave-corpuscle duality, objective reality

OPEN ACCESS

Edited by:
Ana Maria Cetto, National Autonomous University of Mexico, Mexico

Reviewed by:
Xing Lu, Beijing Jiaotong University, China
Kazuharu Bamba, Fukushima University, Japan

***Correspondence:**
Stéphane Avner
stephane.avner@univ-rennes1.fr

Specialty section:
This article was submitted to Mathematical Physics, a section of the journal Frontiers in Physics

Received: *24 March 2020*
Accepted: *19 May 2020*
Published: *17 July 2020*

Citation:
Avner S and Boillot F (2020) Electron Mass Predicted From Substructure Stability in Electrodynamical Model. Front. Phys. 8:213. doi: 10.3389/fphy.2020.00213

INTRODUCTION

Depending on the experiment, the most emblematic subatomic particle, the electron, has been found to interact as a point-like corpuscle in scattering experiments [1], or to behave as an extensible wave [2]. Elaborating on Bohr's interpretation of Quantum Mechanics [3], Heisenberg concluded that particles could neither be represented nor even apprehended by the human mind, and that only their abstract mathematical description existed [4]. For de Broglie however, "abstract presentations have no physical reality. Only the movement of elements localized in space, in the course of time, has physical reality" [5]. Hence, modern physics has identified with unprecedented precision the interactions and their underlying principles, has successfully described its environment, spacetime, but still lacks a characterization of the nature of its "objects," the particles themselves.

Consequently, several kinds of electron models have been proposed: extended models [6], point-like models, and mixed models in which a point-like corpuscle follows an extended trajectory [7]. Early attempts included the *spherical models* of Abraham [8] and Lorentz [9], which led to theories of electromagnetic mass [10–13]. Spherical models soon evolved into the so-called *ring models* of Parson [14], Webster [15], Allen [16], and Compton [17], constituted of rotating

infinitesimal charges and verifying the properties of classical magnetic moment and Compton scattering. Essential constraints however, such as electron cohesion and stability, could not be satisfied: new putative forces, denoted Poincaré stresses [18], were suggested to maintain the cohesion of the negatively charged electron. The abstract descriptions of quantum mechanical theories [19, 20] then successfully accounted for the wave-like behavior of the electron and probabilistically predicted [21] the values of most observables by considering a point-like particle, yet failed at interpreting fundamental constants or explaining how a point-like corpuscle could have spin or a finite energy density. Paradoxically, quantum mechanics revived geometric models when Schrödinger noticed within the Dirac equation itself a rapid oscillatory trembling motion, which he called Zitterbewegung (*zbw*) [22], exhibiting microcurrents arising at light velocity *c*. Surprisingly, the electron seemed to follow a helical trajectory of radius $\lambda\!\!\!^{-}_c$, the reduced Compton wavelength, surrounding the average travel direction (**Figure 1A**). Several such *zbw models*, identifying spin with orbital angular momentum, were interpreted classically [27–29]. Subsequent electrodynamical or hydrodynamical models involved fluids with spin [30], current loops of a certain thickness [31], Dirac-like Equations [32, 33], moving charged membranes [34], plasmoid fibers [35], or toroidal geometry [35, 36]. Wondering whether *zbw* could be a real phenomenon, Hestenes emphasized the need to investigate the electron substructure, suggested *zbw* could originate in the electron self-interaction [37], and showed *zbw* was compatible with the ring models [38].

With the development of realist models of the electron emerged theories of electromagnetic mass. At first, the spherical models of Abraham [8], and Lorentz [9] seemed to fail to recover Einstein's relation $E = mc^2$ due to the appearance of a factor 4/3, but later proved to be compatible, once relativistic corrections were accounted for [12]. Stability of the sphere however still relied on Poincaré stresses or unknown surface tension [34], and electron mass could not be predicted from an objective criterion, but depended on the value taken by an arbitrary parameter, whose value is unconstrained, i.e., the radius of the sphere. Of note, the mass of subatomic particles is not predicted by quantum theories, and their values need to be inserted in calculations [12]. Most ring models [14–17] are prior to the discoveries of the spin, anomalous magnetic moment, and quantum mechanics. The ring model of Bergman and Wesley [31] exhibited cohesion and stability, but the expression for mass still involved an arbitrary parameter (i.e., width of current loop), and the substance constituting the electron remained indeterminate. More recently, Consa proposed a point-like electron following a toroidal trajectory [36], recovered mass independently of any arbitrary parameter, but did not specify how the trajectory developed nor demonstrated its stability. To our knowledge, the Virial theorem, which should be satisfied since the electron is a bound system, has not been considered in electron models. Potential energy is often equated to $+mc^2$, although cohesion potential energy should be negative for a bound system [as it is for the atom for instance [19]]. Kinetic energy is not usually accounted for, even though Lorentz [9], Hestenes [38] and others [e.g., [32]] noted the existence of a rotating motion and wondered whether kinetic energy did not contribute to rest mass. For Barut and Bracken, rest mass energy of the particle is the energy of the internal motion in the rest frame [29].

Hence, several issues remain to be addressed regarding the electron: for instance, which forces could cause the puzzling helical trajectory? What could be the nature of the substance constituting the electron? Could an electrodynamical description account for electron cohesion and stability? And could Lorentz' hypothesis advocating the electromagnetic origin of mass be simultaneously implemented from an objective criterion, instead of an arbitrary parameter?

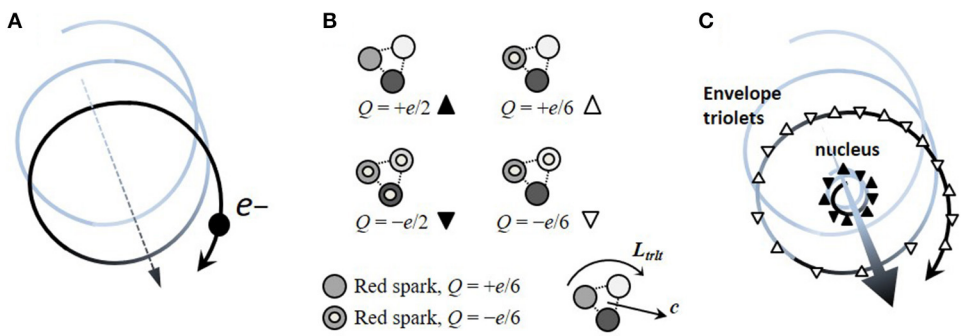

FIGURE 1 | Triolets and the helical trajectory. **(A)** In Schrödinger's Zitterbewegung (*zbw*) model, the wavefunction associated to the electron seems to revolve at light velocity along a helical trajectory of radius $\lambda\!\!\!^{-}_c$, the reduced Compton wavelength, surrounding the average travel direction, and to exhibit microcurrents. Quantum mechanics does not specify which forces could cause the electron, which is assumed to be point-like, to follow such a peculiar helical trajectory. **(B)** Triolets are colorless particles composed of three sparks, each bearing electric charge $\pm e/6$ and a specific strong interaction color charge. Thus triolets bear electric charge $\pm e/6$ or $\pm e/2$ depending on their combination of sparks. They travel at light velocity *c*, possess angular momentum L_{trlt}, and triolets will thereafter be represented as upward or downward, filled or hollow triangles depending on their electric charge, as depicted here. **(C)** In our model, the electron is composed of triolets forming a nucleus and an envelope. It is conceivable that, in the absence of perturbation, the nucleus of the moving electron attracts envelope triolets and maintains them bound, thus explaining their helical trajectory. Conversely, envelope triolets would revolve at light velocity on an orbit of radius $\lambda\!\!\!^{-}_c$ around the nucleus, exhibiting the zbw microcurrents, and guide the nucleus, as in pilot-wave theories [23–26], sensing the electromagnetic fields generated by the envelopes of other particles.

In this study, we present a relativistic electrodynamical model of the electron at rest, in which charged subparticles follow definite trajectories. The model is based on two main hypotheses: (*i*) the existence of charged colorless subparticles called *triolets*, (*ii*) the assumption that triolets revolve at light velocity on coplanar circular orbits, constituting an *envelope* and *nucleus*, depending on their electromagnetic charges. As the electron is coherent, it is assumed that the model satisfies the Virial theorem. Constraints capturing the measured values of several observables (classical and anomalous magnetic moments, spin, Compton wavelength, kinetic energy) are formulated. Using Liénard-Wichert potentials, we then determine the specific kinds and numbers of triolets satisfying envelope and nucleus stability. Remarkably, we find that these kinds and numbers are precisely those that allow predicting electron mass and muon mass electromagnetically directly from the substructure, thus implementing Lorentz' hypothesis. Electron mass is effectively derived from an expression of substructure stability, which constitutes an objective criterion in our view. Our system also illustrates the possibility of constructing causal, local, objective, and realist models of particles beneath the Compton scale. Finally, we discuss novel perspectives suggested by the model, relative to the understanding of wave-corpuscle duality and to its relation to quantum theory.

DESCRIPTION OF THE MODEL AND HYPOTHESES

In a previous study, we proposed that just six kinds of *indestructible* elementary subparticles denoted *sparks*, bearing electric charge $\pm e/6$ and a specific strong interaction color charge, are necessary and sufficient to reconstruct all subatomic particles, so that sparks are conserved and reorganized across particle decays and annihilations [Avner, Boillot, Richard, submitted]. Since sparks are subject to both the strong and electromagnetic interactions, with the former dominating at short distances [20], groups of three sparks could presumably assemble beforehand to form composite colorless particles, thereafter called *triolets*, bearing charge $+e/6$, $-e/6$, $+e/2$, or $-e/2$ (**Figure 1B**). Henceforth, we shall suppose that the electron is exclusively composed of triolets, which travel at light velocity [7], exhibit some intrinsic angular momentum L_{trlt}, and being colorless, are submitted to electromagnetic and centrifugal forces only (hypothesis A).

Following de Broglie's proposition, we aim at constructing a plausible electrodynamical model of the electron at rest, in which positive and negative triolets form an electromagnetically bound system, exhibit the *zbw* microcurrents, and account for all experimentally measured observables. The electron is considered here as a particle of a certain extension, composed of revolving charged subparticles, the triolets, thereby exhibiting magnetic moment and intrinsic angular momentum (its spin) sensed by other particles. We know that the measured value of the electron magnetic moment is the sum of Bohr magneton $\mu_B = -e\hbar/2m$, predicted by both classical physics and quantum mechanics, where $\hbar$ is reduced Planck constant, m the electron mass, and e the elementary charge, and an *anomalous* magnetic moment [39], which accounts for a small fraction $a_{anml} \backsimeq 0.001159$ of the previous and is only predicted by quantum electrodynamics [20]. Remarkably, the value of the classical magnetic moment of the electron can be derived by considering a charge $(-e)$ revolving on a circular orbit of radius $\lambda\!\!\!^{-}_c$ [19]. Hence, we reckoned the classical and anomalous magnetic moments could, respectively, be produced by two different *components* of the electron, namely a negatively charged *envelope* and a neutrally charged *nucleus*, also possibly responsible for the electron's wavelike and corpuscular behaviors, respectively. The peculiar helical trajectory of the electron predicted by *zbw* could then be naturally apprehended by considering that *zbw* describes the dynamics of envelope triolets, which are attracted and bound to the nucleus (**Figure 1C**). Electron spin could correspond to the sum of angular momenta of envelope triolets. Moreover, we shall regard electron mass as being a manifestation of the total electromagnetic cohesion energy E of the particle, as Lorentz hypothesized [9], through Einstein's formula $m = E/c^2$. The latter interpretation of the mass is naturally suggested by the observation that the muon possesses a mass $\sim$206.77 times bigger than that of the electron, while its Compton wavelength is $\sim$206.77 times smaller, as would be the case for a mass of electromagnetic origin, presenting a potential proportional to inverse distance.

The net electromagnetic forces acting on any particular envelope triolet should mostly depend on its surrounding triolets. The envelope could be organized into a complex structure, with triolets irregularly distributed along the orbits, or revolving at various radii, or experiencing fluctuations. To facilitate calculations however, we chose to make approximations and consider triolets at radial equilibrium rotating in the same direction on four coplanar circular orbits of different radii depending on their four different electromagnetic charges (hypothesis B, **Figure 2**). In our model, positive and negative nucleus triolets are intertwined to maintain their cohesion and could rotate along two close yet separate orbits due to the charged envelope. This could cause in turn a similar arrangement in the envelope, which would exhibit predominantly intertwined triolets, in spite of the excess of negative triolets. We are aware our model is only an approximation, even if we reckon that a collection of fluctuating $\pm e/6$ and $\pm e/2$ triolets traveling at light velocity could possibly converge toward such a configuration. Because of their stronger charges, $\pm e/2$ triolets could be more tightly bound and form a condensed nucleus, while $\pm e/6$ triolets would be bound more loosely and constitute the envelope.

In addition, as the electron is a bound system whose inner potentials allegedly depend on position coordinates only and not velocities (justification is given below), the Virial theorem should be verified [40]: for inverse square law electromagnetic interactions, one typically has $E = U/2$ and $E = -T$, where T is the total internal kinetic energy and U the internal potential energy. Therefore, T and U should, respectively, amount to $+mc^2$ and $-2mc^2$, resulting in total internal energy

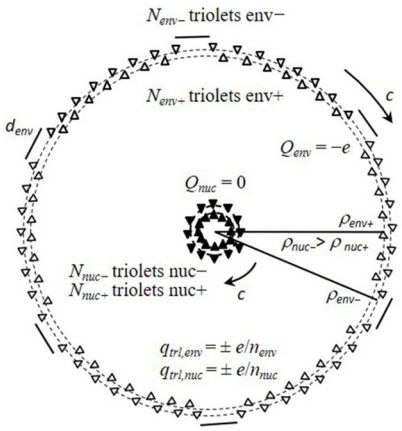

FIGURE 2 | Model of the electron at rest. In our simplified model, triolets rotate at light velocity in the same direction along four different coplanar circular orbits depending on their electric charge, constituting an envelope, and nucleus. Negative triolets are more numerous at the envelope, while the nucleus is neutrally charged. Due to the charged envelope, nucleus triolets are separated into two close orbits depending on their charge. Envelope triolets similarly revolve on separated orbits whose radii are close to the reduced Compton wavelength. Possible triolet configurations (triolet kinds and numbers, angular distributions, orbital radii) must fulfill constraints expressing radial stability and the measured values of charge, spin, magnetic moments, and mass. Due to consecutive negative triolets in the envelope, intertwined envelope triolets assemble into stretches separated by a distance d_{env}.

$E = T + U = -mc^2$ corresponding to electron mass, the minus sign being indicative of a bound system. Finally, we shall admit that, for the electron at rest, envelope triolets approximately follow a circular trajectory of radius $\lambda\!\!\!^{-}_{c} = \hbar/mc$, as suggested by the classical derivation of Bohr's magneton, and by *zbw*-like models. Interpretations of fundamental constants associated to the electron, such as reduced Planck constant $\hbar$ and fine-structure constant $\alpha = e^2/4\pi\varepsilon_0\hbar c$ (where ε_0 designates vacuum permittivity), should also emerge from the model.

FORMULATION OF THE MODEL

Our system captures the measured values of charge, magnetic moments, spin and kinetic energy, and will be validated by showing that cohesion and stability can be satisfied, and potential energy (and thus electron mass) can be recovered. Let us here mathematically formulate the constraints: (*i*) a charge $-e$ carried by $N_{env} = N_{env+} + N_{env-}$ triolets of charge $\pm e/n_{env}$ at the envelope; (*ii*) a classical magnetic moment μ_B generated by envelope triolets rotating at radii $\rho_{env+} = \eta_{env+}\lambda\!\!\!^{-}_{c}$, $\rho_{env-} = \eta_{env-}\lambda\!\!\!^{-}_{c}$, and producing currents I_{env+}, I_{env-}; (*iii*) an anomalous magnetic moment $a_{anml.}\mu_B$ generated by N_{nuc} nucleus triolets ($N_{nuc+} = N_{nuc-}$) of charge $\pm e/n_{nuc}$ rotating in the same direction as envelope triolets at radii $\rho_{nuc+} = \eta_{nuc+}\lambda\!\!\!^{-}_{c}$, $\rho_{nuc-} = \eta_{nuc-}\lambda\!\!\!^{-}_{c}$, with momentum $p_{nuc+} \simeq p_{nuc-} = p_{nuc}$ and producing currents I_{nuc+}, I_{nuc-}; (*iv*) an internal kinetic energy $T = \sum_i p_i c = +mc^2$; (*v*) a spin $S_{env} = +\hbar/2$ generated by envelope triolets of momentum p_{env+}, p_{env-}:

$$-e = e\left[\left(\frac{N_{env+}}{n_{env}}\right) - \left(\frac{N_{env-}}{n_{env}}\right) + \left(\frac{N_{nuc+}}{n_{nuc}}\right) - \left(\frac{N_{nuc-}}{n_{nuc}}\right)\right], \quad (1)$$

$$\frac{-e\hbar}{2m} = I_{env+}\pi\rho_{env+}^2 + I_{env-}\pi\rho_{env-}^2, \quad (2)$$

$$\frac{-a_{anml}e\hbar}{2m} = I_{nuc+}\pi\rho_{nuc+}^2 + I_{nuc-}\pi\rho_{nuc-}^2, \quad (3)$$

$$\sum_i p_i c = \left(N_{env+}p_{env+} + N_{env-}p_{env-} + N_{nuc}p_{nuc}\right)c, \quad (4)$$

$$\frac{\hbar}{2} = N_{env+}\rho_{env+}p_{env+} + N_{env-}\rho_{env-}p_{env-}. \quad (5)$$

The fact that the muon has same spin as the electron, despite possessing a smaller Compton wavelength and the same number of triolets according to our chemical theory [Avner, Boillot, Richard, submitted], suggests that the angular momentum of envelope triolets could be a constant $\rho_{env+}p_{env+} \simeq \rho_{env-}p_{env-} \equiv L_{trlt,env}$, yielding from (5):

$$\hbar = 2N_{env}L_{trlt,env}. \quad (6)$$

$L_{trlt,env}$ is possibly determined by the triangular substructure of envelope triolets made of three strongly interacting sparks, and could be at the basis of Planck's constant. Further constraints are also deduced (see Values of Observables) from Equations (1–5):

$$n_{env} = N_{env-} - N_{env+}, \quad (7)$$

$$n_{env} = \left(N_{env-}\eta_{env-} - N_{env+}\eta_{env+}\right), \quad (8)$$

$$a_{anml}n_{nuc} = N_{nuc+}\left(\eta_{nuc-} - \eta_{nuc+}\right), \quad (9)$$

$$\frac{T_{env} + T_{nuc}}{mc^2} = 1 \simeq \frac{1}{b_{env}}\left(\frac{N_{env+}}{\eta_{env+}} + \frac{N_{env-}}{\eta_{env-}}\right) + \frac{N_{nuc}}{b_{nuc}\eta_{nuc}}, \quad (10)$$

$$b_{env} = 2N_{env}, \quad (11)$$

where b_{env} and b_{nuc} are dimensionless numbers. Assuming that $\eta_{env+} \simeq \eta_{env-} \equiv \eta_{env} \simeq 1$, we deduce (in Values of Observables) from Equations (10–11) that the kinetic energies of the envelope and nucleus are approximately equal $T_{env+} \simeq T_{nuc} \simeq +mc^2/2$, leading to relation:

$$b_{nuc}\eta_{nuc} = 2N_{nuc}. \quad (12)$$

Furthermore, the electromagnetic force acting on a nucleus triolet due to the envelope charge and current and the electromagnetic force exerted on an envelope triolet due to the net nucleus magnetic moment were derived but found to be negligible when compared to intra-component interactions. This suggests that each component is only loosely bound to the other, almost constituting an independent

system, and thus verifies the Virial theorem independently (see Values of Observables), yielding for potential energies $U_{env} \simeq U_{nuc} \simeq -mc^2$ and total energies $E_{env} \simeq E_{nuc} \simeq -mc^2/2$. The system of Equations (9–11) further allows to determine η_{nuc+} (Values of Observables) for each value of N_{nuc+}:

$$\eta_{nuc+} = \frac{N_{nuc+}}{b_{nuc}} \left[2 - \frac{a_{anml} b_{nuc} n_{nuc}}{2N_{nuc+}^2} + \sqrt{4 + \left(\frac{a_{anml} b_{nuc} n_{nuc}}{2N_{nuc+}^2} \right)^2} \right], \tag{13}$$

while η_{nuc-} is then given by Equation (9).

System cohesion and stability can be formulated by ensuring triolets are at radial equilibrium. As triolets are electrically charged and travel at light velocity, we use Liénard-Wichert potentials from relativistic electrodynamics [41] to express the radial components of electric field $\boldsymbol{E_{ij\perp}}$ and magnetic field $\boldsymbol{B_{ij}}$ emitted by triolet T_j of charge q_j at retarded time t', radius ρ_j and retarded angle θ'_j, and sensed at distance R_{ij}—electromagnetic fields traveling at light velocity in vacuum—by triolet T_i arriving at the vertical (angle 0), radius ρ_i, at time t (**Figure 3A**). From known electrodynamical expressions [41] for these fields, using cylindrical unit vectors and coordinates, and **Figure 3B**, we deduce (Forces and Potentials):

$$\mathbf{E_{ij\perp}} = \frac{q_j \sin\gamma_j}{4\pi\varepsilon_0 R_{ij}\rho_i \left(1+\sin\gamma_j\right)^2} \hat{\boldsymbol{\rho}}, \tag{14}$$

$$\mathbf{B_{ij}} = \frac{-q_j}{4\pi\varepsilon_0 c R_{ij}\rho_j \left(1+\sin\gamma_j\right)^2} \hat{\mathbf{z}}, \tag{15}$$

where R_{ij} and γ_j are defined by:

$$R_{ij}^2 = \rho_i^2 + \rho_j^2 - 2\rho_i\rho_j \cos\theta_j', \tag{16}$$

$$\sin\gamma_j = \frac{\rho_i}{R_{ij}} \sin\theta_j'. \tag{17}$$

Note that these fields depend on position coordinates only, not velocities, thereby justifying the use of the Virial theorem. We then derive expressions (Forces and Potentials) for the net radial Lorentz force $\boldsymbol{F_{ij\perp}}$ due to triolet T_j exerted on triolet T_i belonging to the same component, and for the centrifugal force $\boldsymbol{F}_{ctfg,i}$ experienced by triolet T_i:

$$\mathbf{F_{ij\perp}} = \frac{q_i q_j}{4\pi\varepsilon_0 R_{ij}\left(1+\sin\gamma_j\right)^2} \left[\frac{\sin\gamma_j}{\rho_i} + \frac{1}{\rho_j} \right] \hat{\boldsymbol{\rho}}, \tag{18}$$

$$\overrightarrow{\mathbf{F}}_{ctfg,i} = \frac{hc}{b_i \rho_i^2} \hat{\boldsymbol{\rho}}, \tag{19}$$

where b_i stands for b_{env} (respectively, b_{nuc}) when T_i belongs to the envelope (resp. the nucleus). In the electron at rest, assuming triolets remain at radial equilibrium, the net radial component of the Lorentz force exerted by other triolets should compensate the centrifugal force. Neglecting the small contribution of the envelope onto the nucleus and vice-versa, and expressing equilibrium for triolet T_i along the radial direction

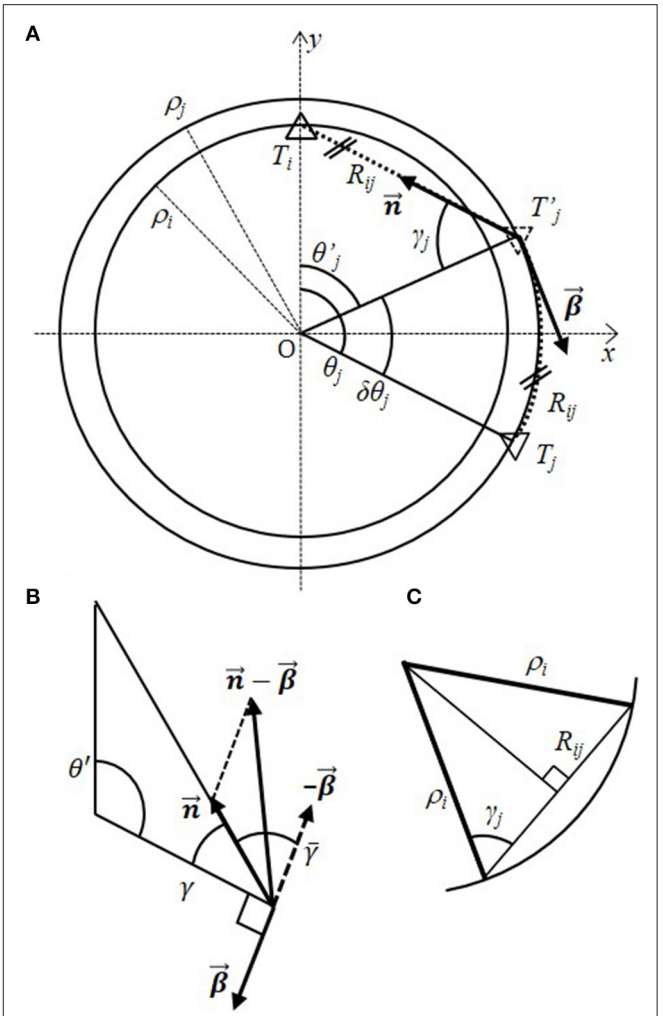

FIGURE 3 | Geometric diagrams. **(A)** The influence of electromagnetic fields due to triolet T_j onto T_i: let triolets T_i and T_j belong to the same component (envelope or nucleus). Triolet T_j rotates at light velocity along circular orbit of radius ρ_j and arrives at angle θ_j at time t, but was at position T_j' at retarded angle θ_j' and time t' when it emitted electromagnetic fields that reached triolet T_i revolving along coplanar circular orbit of radius ρ_i and arriving at angle 0 (vertical y axis) at time t. The retarded electromagnetic fields can be expressed using Liénard-Wichert potentials. This figure applies to all envelope and nucleus triolets. **(B)** Diagram showing vectors and angles involved in the demonstration of the expressions of electromagnetic fields and potentials. **(C)** Diagram depicting the case $\rho_j = \rho_i$.

and rearranging (Triolets at Radial Equilibrium), we obtain for the envelope and nucleus:

$$\frac{1}{\alpha} \simeq \frac{-b_{env}}{n_{env}^2} \sum_{j\in env}^{N_{env}-1} \frac{\rho_i^2 \mathrm{sgn}\left(i\cdot j\right)}{R_{ij}\left(1+\sin\gamma_j\right)^2} \left(\frac{\sin\gamma_j}{\rho_i} + \frac{1}{\rho_j} \right) \equiv G_{i\in env}\left(\eta_i\right), \tag{20}$$

$$\frac{1}{\alpha} \simeq \frac{-b_{nuc}}{n_{nuc}^2} \sum_{j\in nuc}^{N_{nuc}-1} \frac{\rho_i^2 \mathrm{sgn}\left(i\cdot j\right)}{R_{ij}\left(1+\sin\gamma_j\right)^2} \left(\frac{\sin\gamma_j}{\rho_i} + \frac{1}{\rho_j} \right) \equiv G_{i\in nuc}\left(\eta_i\right), \tag{21}$$

where sgn(i·j) is the sign of the product of the charges of triolets T_i and T_j, and α is the fine-structure constant, which is found to be related to the ratio between the centrifugal force and the net radial electromagnetic force experienced by any single triolet inside the electron. We assume positive and negative triolets are intertwined and uniformly distributed along the orbits except—as negative triolets are more numerous at the envelope—consecutive negative envelope triolets, which presumably repel to produce stretches of alternatively charged triolets separated by empty space (**Figure 2**). Let d_{env} designate the distance (using the number of missing triolets as units) between the stretches. The expressions under the sums in Equations (20–21) can be calculated by first considering the non-retarded angular positions θ_j of triolets distributed along the circular orbit, then by determining the corresponding retarded angles θ'_j, as illustrated in Retarted Angles, using Newton's recursion method for instance onto transcendental equation:

$$\left(\theta_j - \theta_j^{'}\right)^2 = 1 - 2\frac{\rho_i}{\rho_j}\cos\theta_j^{'} + \left(\frac{\rho_i}{\rho_j}\right)^2, \tag{22}$$

and then deriving γ_j from Equation (17). Equations (20–21) will help us derive adequate values for N_{env}, N_{nuc}, n_{env}, n_{nuc}, b_{env}, b_{nuc}.

The potential energy due to interactions between the nucleus and envelope being negligible, the total potential energy of our system is approximately $U_{tot} \simeq U_{env} + U_{nuc}$, where U_{env}, and U_{nuc} are, respectively, the envelope and nucleus potential energies, which are evaluated in Potential Energy:

$$U_{env} \simeq \frac{2\alpha mc^2}{n_{env}^2}\sum_{i\in env}^{N_{env}}\sum_{j\neq i}^{N_{env}-1}\frac{\mathrm{sgn}\left(i\cdot j\right)}{H_{ij}\left(1+\sin\gamma_j\right)}, \tag{23}$$

$$U_{nuc} \simeq \frac{2\alpha mc^2}{n_{nuc}^2}\sum_{i\in nuc}^{N_{nuc}}\sum_{j\neq i}^{N_{nuc}-1}\frac{\mathrm{sgn}\left(i\cdot j\right)}{H_{ij}\left(1+\sin\gamma_j\right)}, \tag{24}$$

where $H_{ij} = R_{ij}/\lambda_c$. Assuming $\eta_{env+} \simeq \eta_{env-} \simeq 1$, we demonstrate (Potential Energy) from b_{env}=$2N_{env}$ (11) and Equation (20), which expresses the radial stability of every envelope triolet, that Equation (23) yields $U_{env} \simeq -mc^2$. Likewise, assuming $\eta_{nuc+} \simeq \eta_{nuc-}$, we demonstrate (Potential Energy) from $b_{nuc}\eta_{nuc} = 2N_{nuc}$ (12) and Equation (21), which expresses the radial stability of every nucleus triolet, that Equation (24) yields $U_{nuc} \simeq -mc^2$. Hence, we find: $U_{tot} \simeq U_{env} + U_{nuc} \simeq -2mc^2$, as expected from the Virial theorem, and recover electron mass. As substructure stability implies radial equilibrium for all envelope and nucleus triolets (20–21), it allows predicting electron mass. We find it remarkable that the same number of triolets allows to recover both substructure stability and electron mass.

DETERMINATION OF SUITABLE CONFIGURATIONS

The problem then reduces to determining triolet configurations, i.e., sets of values for {n_{env}, n_{nuc}, N_{env+}, N_{env-}, N_{nuc}, b_{env}, b_{nuc}, η_{env+}, η_{env-}, η_{nuc+}, η_{nuc-}, d_{env}}, that verify radial equilibrium for every triolet and correctly predict the total energy. We shall estimate the stability and total energy in three different models of the envelope successively, each lying at a different level of approximation. The three models are: the *one-orbit* model, where all envelope triolets rotate on the same orbit $\eta_{env+} \simeq \eta_{env-} \equiv \eta_{env}$; the *two-orbits* model, where positively-charged envelope triolets revolve on orbit of radius η_{env+} and negative triolets at radius η_{env-}; the *n-orbits* model where every envelope triolet i rotates on a circular orbit of specific but fixed radius η_i.

We shall first estimate the number of triolets N_{env} present in the envelope by considering the one-orbit model. Assuming $\eta_{env+} \simeq \eta_{env-}$ and $\eta_{nuc+} \simeq \eta_{nuc-}$, we have $R_{ij} \simeq 2\rho_i\cos\gamma_j$ (**Figure 3C**) both at the envelope and nucleus, and Equations (20–21) can be approximated to:

$$\frac{1}{\alpha} \simeq \frac{-b_{env}}{2n_{env}^2}\sum_{j\in env}^{N_{env}-1}\frac{\mathrm{sgn}\left(i\cdot j\right)}{\cos\gamma_j\left(1+\sin\gamma_j\right)} \simeq G_{i\in env}\left(\eta_i\right), \tag{25}$$

$$\frac{1}{\alpha} \simeq \frac{-b_{nuc}}{2n_{nuc}^2}\sum_{j\in nuc}^{N_{nuc}-1}\frac{\mathrm{sgn}\left(i\cdot j\right)}{\cos\gamma_j\left(1+\sin\gamma_j\right)} \simeq G_{i\in nuc}\left(\eta_i\right). \tag{26}$$

Recalling that b_{env} is related to N_{env} via $b_{env} = 2N_{env}$ (11), and setting values for input parameters {n_{env}, d_{env}}, the iteration over N_{env} values in Equation (25) enabled us to determine values for b_{env} and N_{env} approximately verifying Equations (25) and (11) simultaneously. Due to the asymmetry in the arrangement of envelope triolets, we found these Equations were satisfied for different values of N_{env} depending on the triolet T_i under consideration. In the case $n_{env} = 6$, $d_{env} = 0$ for instance, we found positive triolets approximatively satisfied these conditions for $N_{env} \simeq 108$, while negative triolets did so for $N_{env} \simeq 144$, thus justifying the necessity of considering two distinct orbits in the envelope. Although these figures should be regarded as merely indicative, cases $d_{env} = 1$ and $d_{env} = 2$ also pointed at average value $N_{env} = 126$, corresponding to $N_{env+} = 60$ and N_{env-}= 66, and we shall be considering only this case in the remainder of our analysis. For the nucleus, in the absence of a constraint like Equation (11), values for b_{nuc} and η_{nuc} satisfying Equations (26) and (12) simultaneously were determined for every iterated value of N_{nuc}. However, when accounting for the correction due to envelope current (first two terms, Triolets at Radial Equilibrium):

$$G_{env>i\in nuc} \approx \frac{b_{nuc}\mathrm{sgn}\left(i\right)}{n_{nuc}}\left[\frac{\eta_{nuc}^3}{2} + \frac{3\eta_{nuc}^4}{8}\right], \tag{27}$$

the best estimate appeared to be $N_{nuc} = 18$ (**Table 1**). Note that input values other than $n_{env} = 6$, $n_{nuc} = 2$ did not yield any possible solutions.

Now, considering $n_{env} = 6$, $n_{nuc} = 2$, $d_{env} = 2$, $\eta_{env+} \simeq \eta_{env-} \simeq 1$ (one-orbit model), and putting in the value obtained above for N_{env}, we evaluated potential energies U_{env}, U_{nuc} using Equations (13, 23–24) and found $U_{env} = -0.997{\cdot}mc^2$ (**Table 2**), $U_{nuc} \simeq -1.000{\cdot}mc^2$ (**Table 1**). The total potential energy therefore amounts to $U_{tot} \simeq -1.997{\cdot}mc^2$, close to our expected result. Hence, recalling that kinetic energies satisfy $T_{env} \simeq T_{nuc} \simeq$

TABLE 1 | Stability and energy of various nucleus configurations.

N_{nuc}	b_{nuc}	η_{nuc+}	η_{nuc-}	G_{nuc+}	G_{nuc-}	$G_{env>nuc}$	U_{nuc}	T_{nuc}
6	553.42	0.0213	0.0221	127.69	146.51	±0.001	−0.9996	+0.5001
8	425.49	0.0373	0.0379	132.47	141.62	±0.006	−0.9998	+0.4999
12	290.89	0.0823	0.0827	135.02	138.21	±0.043	−1.0000	+0.5000
16	221.03	0.1446	0.1449	136.29	137.78	±0.186	−1.0002	+0.5001
18	197.35	0.1823	0.1825	136.49	137.58	±0.340	−1.0005	+0.5000
20	178.27	0.2243	0.2245	136.63	137.45	±0.588	−0.9999	+0.5000
22	162.55	0.2706	0.2708	136.71	137.35	±0.970	−1.0003	+0.4999
24	149.39	0.3212	0.3214	136.79	137.29	±1.538	−1.0000	+0.5000

At the nucleus, setting $n_{nuc} = 2$, values for b_{nuc} and nucleus radii η_{nuc+}, η_{nuc-} are determined for several values of N_{nuc}, the number of nucleus triolets, according to Equations (9, 12, 13, 26), so as to yield $U_{nuc} \simeq -mc^2$, $T_{nuc} \simeq +mc^2/2$ and satisfactory stability values G_{nuc+}, G_{nuc-} (value 137.03 stands for stability). Accounting for first correction terms $G_{env>nuc}$ due to envelope current and specified by Equation (27), the best estimate seems to be $N_{nuc} = 18$. Nucleus potential energy U_{nuc} and kinetic energy T_{nuc} are expressed in terms of mc^2.

TABLE 2 | Stability and energy of various envelope models.

Model	η_{env+}	η_{env-}	N_{env}	$<G_i>$	K	U_{env}	T_{env}
One orbit	1.0	1.0	120	131.4	41.7	−0.949	+0.5000
			126	136.7	48.0	−0.996	+0.5000
			132	157.5	46.5	−1.139	+0.5000
Two fixed orbits	0.977	1.023	120	124.6	17.3	−0.962	+0.4997
			126	130.0	16.1	−1.011	+0.4997
			132	148.7	16.1	−1.155	+0.4997
Specific orbits	various	various	126	137.7	3.2	−0.975	+0.5020

The potential energy U_{env}, kinetic energy T_{env}, and average absolute stability deviation K are shown for the three considered envelope models, involving triolets revolving on (i) a single orbit at reduced Compton wavelength, (ii) two fixed envelope orbits η_{env+} and η_{env-}, (iii) N_{env} orbits of specific but fixed radii, with parameters set to $n_{env} = 6$, $d_{env} = 2$. Energies are expressed in terms of mc^2, where m is the mass of the electron and c is light velocity. It can be seen that for the single orbit and two fixed orbits models, the solution $N_{env+} = 60$, $N_{env-} = 66$ yields accurate potential energy values. Although in the one-orbit or two-orbits models, total energy of the envelope E_{env} is close to $-mc^2/2$, K stability values strongly diverge from 0, indicating that triolets do not verify radial equilibrium. A configuration of fixed specific orbits yielding overall satisfactory energy and average stability values (value 137.03 stands for stability) has been determined using our optimization algorithm.

TABLE 3 | Stability of individual envelope triolets.

Triolet		One orbit		Two fixed orbits		Specific orbits	
#	+/−	η_i	G_i	η_i	G_i	η_i	G_i
1	−	1.0	75.4	1.023	108.4	1.761	137.0
2	+	1.0	189.4	0.977	145.4	0.861	114.0
3	−	1.0	105.2	1.023	134.5	0.880	137.0
4	+	1.0	178.8	0.977	134.3	0.931	139.5
5	−	1.0	110.4	1.023	139.7	0.915	137.0
6	+	1.0	176.0	0.977	131.3	0.947	145.3
7	−	1.0	111.9	1.023	141.1	0.925	137.3
8	+	1.0	175.4	0.977	130.7	0.958	137.0
9	−	1.0	111.8	1.023	141.0	0.987	143.6
10	+	1.0	176.0	0.977	131.4	0.974	137.0
11	−	1.0	110.6	1.023	139.7	1.012	142.0
12	+	1.0	177.8	0.977	133.2	0.977	141.7
13	−	1.0	108.2	1.023	137.1	0.968	143.1
14	+	1.0	181.0	0.977	136.5	0.975	137.0
15	−	1.0	103.9	1.023	132.5	1.019	137.5
16	+	1.0	186.7	0.977	142.3	0.998	137.0
17	−	1.0	96.1	1.023	124.0	1.045	137.0
18	+	1.0	198.2	0.977	154.0	1.004	144.0
19	−	1.0	78.0	1.023	104.4	1.017	133.8
20	+	1.0	231.7	0.977	188.2	1.043	137.0
21	−	1.0	−12.0	1.023	1.0	1.130	137.0
K			48.0		16.1		3.2

*The stability of individual envelope triolets belonging to the first stretch—the five other stretches of 21 triolets being identical in the $N_{env} = 126$ case—is evaluated by determining G_i and comparing it to $1/\alpha \simeq 137.036$, in the three envelope models (single orbit, two fixed orbits, n fixed orbits of specific radii), with input parameters set to $n_{env} = 6$, $N_{env+} = 60$, $N_{env-} = 66$, $d_{env} = 2$. The one-orbit model was evaluated at η_{env}=1 corresponding to radius $\lambda\!\!\!^{-}_c$, the reduced Compton wavelength. The two-orbits model was evaluated for radii $\eta_{env+} = 0.977$, $\eta_{env-} = 1.023$, that yielded acceptable energy value (**Table 2**). In the model with specific radii, our optimization algorithm converged toward the 21 different radii shown here, together with their corresponding individual stability value G_i (value 137.03 stands for stability). The average absolute deviation K to $1/\alpha$ is supplied for the three envelope models.*

$+mc^2/2$, then $T_{tot} \simeq T_{env} + T_{nuc} \simeq +mc^2$, $E_{tot} \simeq T_{tot} + U_{tot} \simeq -mc^2$, and the mass of the electron is deduced directly from our model substructure. Likewise, since the muon is seen as an excited state of the electron [6] according to our chemical theory [Avner, Boillot, Richard, submitted], presumably displaying a similar arrangement of triolets albeit on a smaller scale, muon mass can also be successfully calculated by replacing m by muon mass m_μ in expressions (23–24), or equivalently $\lambda\!\!\!^{-}_c$ by the reduced muonic Compton Wavelength $\lambda\!\!\!^{-}_{\mathrm{muon}}$.

We next evaluated the cohesion and stability of individual triolets. For the symmetric nucleus, we computed the right-hand side G_{nuc} of Equation (21) for every triolet; for $n_{nuc} = 2$, $N_{nuc} = 18$ for instance, accounting for the correction due to the envelope current, we obtained $G_{nuc}(\eta_{nuc+}) \simeq 136.83$, $G_{nuc}(\eta_{nuc-}) \simeq 137.24$ (**Table 1**). For the asymmetric envelope, which can be divided into six identical stretches of 21 triolets in the case $N_{env} = 126$, we computed the right-hand sides G_{env} of Equation (20) for every triolet belonging to the first stretch and compared the results with the left-hand side $1/\alpha \simeq 137.036$, which they should yield if triolets were truly at radial equilibrium. For the one-orbit model, setting $n_{env} = 6$, values of G_{env} disagreed with the expected value for all values of d_{env} (the case $d_{env} = 2$ is given in **Table 3**). Clearly, in these conditions at least, the centrifugal and net electromagnetic forces fail to compensate and to ensure radial equilibrium, one dominating over the other, and triolets would be moving radially as well as azimuthally. Therefore, we considered the two-orbits model with $\eta_{env+} \simeq 0.977$, $\eta_{env-} \simeq 1.023$, for which we obtained an acceptable energy value (**Table 2**). Once again, we found that radial equilibrium was not verified for many envelope triolets, especially for consecutive negative triolets or those adjacent to them (**Table 3**). Hence, we decided to complicate our model again and considered envelope triolets orbiting at various but fixed radii ρ_i (n-orbits model) instead of the probably too general ρ_{env+} and ρ_{env-}. We heuristically determined fixed radii exhibiting reasonable stability

for all envelope triolets, then used an optimization algorithm, described in Optimization Algorithm, to make every triolet tend toward radial equilibrium, minimizing criterion K, the average absolute deviation from $1/\alpha$ per triolet:

$$K = \frac{1}{N_{env}} \sum_{i}^{N_{env}} \left| G_{i \in env}(\eta_i) - \frac{1}{\alpha} \right|, \tag{28}$$

which effectively constitutes a measure of global stability of envelope triolets. Our algorithm converged toward a solution yielding acceptable energy and global stability (**Table 2**). The stability values $G_{env}(\eta_i)$ of individual envelope triolets belonging to the first stretch in the n-orbits model are shown in **Table 3**: most values appeared to be close to $1/\alpha$. We found that our optimization algorithm nicely converged toward stable solutions. However, the latter were highly dependent on initial conditions, and a thorough optimization study is needed to ensure local minima are avoided.

DISCUSSION

In this study, we presented a relativistic electrodynamical model of the electron based on natural interpretations of its associated observables. Our electron model is composed of triolets that revolve along coplanar circular orbits constituting an envelope and nucleus, which could be responsible for its wavelike and corpuscular behaviors, respectively. These two components would thus constitute a natural solution to wave-corpuscle duality. Capturing the values of charge, spin, magnetic moments, Compton wavelength and kinetic energy, we created a triolet-based configuration that verified cohesion and stability without invoking Poincaré stresses, and predicted electron and muon mass, defined as electromagnetic cohesion energy, directly from substructure stability. Importantly, our model accounts for kinetic energy and presents a negative cohesion potential energy, in agreement with the Virial theorem. In our model, the numbers of triolets in the envelope and nucleus are the adjusting parameters, and the same numbers are found to account both for substructure stability and electron mass. Notably, electron mass can be derived directly from an expression of substructure stability. Our study therefore implements Lorentz' hypothesis, which advocates the electromagnetic origin of mass, from an objective criterion, even if satisfaction of the criterion itself relies on two parameters, i.e., the numbers of triolets in the envelope and nucleus. Noteworthy, these parameters are not arbitrary, but instead are strongly constrained by several relations (11, 12, 20, 21, 27) that fix their values in our model. Altogether, we believe our study establishes that deterministic electrodynamical models of subatomic particles can be constructed beneath the Compton scale, in agreement with an objectively realist conception of physics.

Envelope triolets could also fluctuate radially or otherwise in time, possibly constituting a periodic wave that revolves at light velocity. This system has not been investigated here, but is of interest because this periodic wave could correspond to the wave associated to the electron, first imagined by de Broglie and later represented by wavefunction $|\psi>$ in Schrödinger's wave mechanics or Dirac's quantum mechanics. It is conceivable that a wave made of envelope triolets, if it exists, attracts and drives the nucleus in the manner of the de Broglie-Bohm guiding wave [23, 24], sensing the electromagnetic fields generated by the envelopes belonging to other particles. Hence, envelope triolets could undulate and incarnate wavefunction $|\psi>$, whose concrete existence has recently been reconsidered [42]. Note further that nucleus triolets could also form a wave, reminiscent of the second wave described in de Broglie's double solution theory [23]. Specifically, triolets could propagate in a highly dynamical manner and experience irregular fluctuations, as in the hydrodynamical model of Bohm and Vigier [25]. Importantly, it has been suggested that solutions of this type could account both for quantum phenomena [26] and for quantum principles [37]. Bell also wrote that such solutions were compatible with the predictions of quantum mechanics [43]. Further, it is conceivable that such a complex envelope can exhibit several stable states, much like modes for a vibrating rope. These could correspond to the eigenstates of quantum mechanics. In the general case, the envelope would be in an unstable state, but could converge toward one of its eigenstates upon measurement, which could be conceived as the sum of interactions between system subparticles and apparatus subparticles. Such propositions constitute an interpretation of von Neumann's *reduction of the wave packet* [44], and would provide a possible solution to *the measurement problem* of quantum mechanics [45].

These considerations suggest that quantum theories, which encompass all subatomic phenomena and whose standard interpretation states that everything is intrinsically probabilistic, could eventually emerge [46, 47] from a relativistic electrodynamical description in agreement with the deterministic paradigm, which supports the causality principle, objective reality, and governs macroscopic physics. In this perspective, Schrödinger and Dirac Equations would constitute high-level descriptions of the dynamics of envelope triolets. Our study therefore provides new insight regarding the unification of the two apparently irreconcilable paradigms in physics: the deterministic and quantum paradigms.

Now, how exactly does the electron appear to be point-like in corpuscular interactions? How does our model relate to the observation that the electron seems spherical [48], or that its spin, charge and orbital components seem to be separable [49–51]? How would the moving electron, which exhibits a wave satisfying de Broglie relation $p=h/\lambda$, be described? Could our description be regarded as an attempt to create a corpuscular counterpart to wave mechanics? Could analogous electrodynamical models be similarly constructed for other subatomic particles [52]? Could our extended model of the electron bring insight to the nature of molecular bonding, or to the arrangement of electrons inside atoms? And finally, what would be the implications for the interpretation of quantum mechanics [45]? How would quantum properties, such as the existence of eigenstates, the measurement problem or entanglement, and quantum phenomena, such as the two-slits experiment or the one-dimensional potential well, be understood in the light of our model? We believe the

aforementioned questions should stimulate discussion and foster novel investigations.

METHODS

Values of Observables

Charge

The charge of the electron is given by the N_{env+} triolets of charge $(+e/n_{env})$, the N_{env-} triolets of charge $(-e/n_{env})$, the N_{nuc+} triolets of charge $(+e/n_{nuc})$ and the N_{nuc-} triolets of charge $(-e/n_{nuc})$:

$$-e = e\left[\left(\frac{-N_{env-}}{n_{env}}\right) + \left(\frac{N_{env+}}{n_{env}}\right) + \left(\frac{-N_{nuc-}}{n_{nuc}}\right) + \left(\frac{N_{nuc+}}{n_{nuc}}\right)\right].$$

Assuming the nucleus is neutrally charged (hypothesis B), implying $N_{nuc+} = N_{nuc-}$, we deduce:

$$n_{env} = N_{env-} - N_{env+}. \tag{A1}$$

Nucleus and Envelope Orbits

Let us suppose triolets of charges $(+e/n_{env})$, $(-e/n_{env})$, $(+e/n_{nuc})$, $(-e/n_{nuc})$ revolve along four coplanar circular orbits of radii:

$$\begin{cases} \rho_{env+} = \eta_{env+}\lambda\!\!\!^{-}_{C} \\ \rho_{env-} = \eta_{env-}\lambda\!\!\!^{-}_{C} \\ \rho_{nuc+} = \eta_{nuc+}\lambda\!\!\!^{-}_{C} \\ \rho_{nuc-} = \eta_{nuc-}\lambda\!\!\!^{-}_{C} \end{cases} \tag{A2}$$

where $\lambda\!\!\!^{-}_{c} = \hbar/mc$ is the reduced Compton wavelength, and η's are dimensionless real numbers.

Classical and Anomalous Magnetic Moments

Let us express the classical magnetic moment $\mu_B = -e\hbar/2m = \sum_i I_i A_i = \sum_i Q_i A_i/t_i$, where I_i is the current generated by triolet T_i, Q_i its charge, $t_i = c/2\pi\rho_i$ the time taken to go through a full orbit at light velocity c, and A_i the area formed by this orbit. The magnetic moment is due to a net charge $(-e)$ made of $N_{env} = N_{env+} + N_{env-}$ triolets revolving in the same direction along envelope orbits of radii ρ_{env+} and ρ_{env-}:

$$\begin{aligned} \mu_B &= \frac{-e\hbar}{2m} = \frac{Q_{env+}A_{env+}}{t_{env+}} + \frac{Q_{env-}A_{env-}}{t_{env-}}, \\ \frac{-e\hbar}{2m} &= \frac{N_{env+}e}{n_{env}}\frac{c\pi\,\rho_{env+}^2}{2\pi\rho_{env+}} + \frac{N_{env-}(-e)}{n_{env}}\frac{c\pi\rho_{env-}^2}{2\pi\rho_{env-}}, \\ \frac{-e\hbar}{2m} &= \frac{ec}{2n_{env}}\left(N_{env+}\eta_{env+} - N_{env-}\eta_{env-}\right)\frac{\hbar}{mc}, \\ &\left(N_{env-}\eta_{env-} - N_{env+}\eta_{env+}\right) = n_{env}. \end{aligned} \tag{A3}$$

As the anomalous magnetic moment $\mu_{nuc} = -a_{anml}(e\hbar/2m)$, with $a_{anml} \simeq 0.001159$, is relatively small, let us assume it is produced by an equal number $N_{nuc+} = N_{nuc-}$ of positive and negative triolets of charge $(\pm e/n_{nuc})$ revolving in the same direction as envelope triolets along nucleus orbits of slightly different radii due to the net envelope charge:

$$\mu_{nuc} = -a_{anml}\frac{e\hbar}{2m} = \frac{Q_{nuc+}A_{nuc+}}{t_{nuc+}} + \frac{Q_{nuc-}A_{nuc-}}{t_{nuc-}},$$

$$N_{nuc+}\left(\eta_{nuc-} - \eta_{nuc+}\right) = a_{anml}n_{nuc}. \tag{A4}$$

Virial Theorem

The virial theorem states that if a system remains bound, and if its inner potentials do not depend on velocities but only on positions, then the kinetic and potential energies take on definite shares in the total energy, depending on the degree n of the forces that apply. As the electron is a bound system, and as in our system the magnetic force will be found to depend on position coordinates ρ and γ only, the theorem applies and, for electromagnetic interactions in r^{-2}, it stipulates that:

$$\begin{cases} T = mc^2 \\ U = -2mc^2 \\ E = T + U = -mc^2 \end{cases} \tag{A5}$$

where T, U, and E, respectively, designate the internal kinetic energy, internal potential energy, and total internal energy of the system. Note that the potential and total energies are negative, as they should be for a bound system.

Kinetic Energy

The kinetic energy is given by:

$$\begin{aligned} T = mc^2 \;&=\; \sum_i p_i c = N_{env+}p_{env+}c + N_{env-}p_{env-}c \\ &+\; N_{nuc+}p_{nuc+}c + N_{nuc-}p_{nuc-}c, \end{aligned} \tag{A6}$$

suggesting:

$$\begin{cases} p_{env+} = mc/K_{env+} \\ p_{env-} = mc/K_{env-} \\ p_{nuc+} = mc/K_{nuc+} \\ p_{nuc-} = mc/K_{nuc-} \end{cases}, \tag{A7}$$

where the K's remain to be determined, thus yielding from Equation (A6):

$$1 = \frac{N_{env+}}{K_{env+}} + \frac{N_{env-}}{K_{env-}} + \frac{N_{nuc+}}{K_{nuc-}} + \frac{N_{nuc+}}{K_{nuc-}}. \tag{A8}$$

Note that we may assume that nucleus triolets possess comparable momentum $p_{nuc+} \simeq p_{nuc-} = p_{nuc}$, and that their orbit radius is approximately $\rho_{nuc+} \simeq \rho_{nuc-} = \rho_{nuc}$, since $(\rho_{nuc+} - \rho_{nuc-})$ is very small according to Equation (A4).

Spin

Since particles as different as quarks and leptons (which possess different numbers of sparks according to our chemical model [Avner, Boillot, Richard, submitted]) share same spin, the latter can be interpreted as being the total angular momentum the particle conveys to the objects it encounters, i.e., the sum of the angular momenta of its envelope triolets. For the electron, assuming all triolets revolve in the same positive direction, it is written using Equations (A2, A6):

$$S = +\frac{\hbar}{2} = \sum_i \rho_i p_i = N_{env+}\rho_{env+}p_{env+} + N_{env-}\rho_{env-}p_{env-}, \tag{A9}$$

$$\frac{1}{2} = \frac{N_{env+}\eta_{env+}}{K_{env+}} + \frac{N_{env-}\eta_{env-}}{K_{env-}}, \tag{A10}$$

Further, as the muon is composed of the same number of triolets as the electron according to our chemical model and exhibits a Compton length much smaller than that of the electron [Avner, Boillot, Richard, submitted], spin $\hbar/2$ is thus independent of the radii of triolets' orbits. A necessary and sufficient condition is then that variables K's be proportional to η's:

$$\begin{cases} K_{env+} = b_{env+}\eta_{env+} \\ K_{env-} = b_{env-}\eta_{env-} \\ K_{nuc+} = b_{nuc}\eta_{nuc+} \\ K_{nuc-} = b_{nuc}\eta_{nuc-} \end{cases} \tag{A11}$$

where b_{env+}, b_{env-}, b_{nuc+}, b_{nuc-} are values independent of radii, in order that the η's cancel out in Equation (A10), yielding:

$$\frac{1}{2} = \frac{N_{env+}}{b_{env+}} + \frac{N_{env-}}{b_{env-}}. \tag{A12}$$

The angular momentum of triolet i is given by:

$$L_i = p_i\rho_i = \frac{mc}{b_i\eta_i} \cdot \eta_i\frac{\hbar}{mc} = \frac{\hbar}{b_i}, \tag{A13}$$

implying for spin and kinetic energy:

$$\frac{b_{env}}{2} = N_{env+} + N_{env-}, \tag{A14}$$

$$1 = \frac{N_{env+}}{b_{env}\eta_{env+}} + \frac{N_{env-}}{b_{env}\eta_{env-}} + \frac{N_{nuc+}}{b_{nuc}\eta_{nuc+}} + \frac{N_{nuc-}}{b_{nuc}\eta_{nuc-}}. \tag{A15}$$

Definition of Planck's Constant

Supposing angular momentum $L_{trlt,env}$ is a constant common to every envelope triolet, the expression for the spin, from Equation (A9), due to the envelope is:

$$\frac{\hbar}{2} = N_{env+}L_{trlt,env} + N_{env-}L_{trlt,env} = N_{env}L_{trlt,env},$$

and thus:

$$\hbar = 2N_{env}L_{trlt,env}, \tag{A16}$$

meaning that the constant angular momentum $L_{trl,env}$ common to every envelope triolet could be at the basis of Planck's constant.

Kinetic Energy of the Nucleus and Envelope

From Equations (A6, A7, A11), the kinetic energy of the nucleus is given by:

$$\begin{aligned} T_{nuc} &= N_{nuc+}p_{nuc+}c + N_{nuc-}p_{nuc-}c \\ &= \frac{mc^2N_{nuc+}}{b_{nuc}}\left(\frac{1}{\eta_{nuc+}} + \frac{1}{\eta_{nuc-}}\right). \end{aligned} \tag{A17}$$

Likewise, the kinetic energy of the envelope is:

$$T_{env} = N_{env+}p_{env+}c + N_{env-}p_{env-}c,$$

$$T_{env} = \frac{mc^2}{b_{env}}\left(\frac{N_{env+}}{\eta_{env+}} + \frac{N_{env-}}{\eta_{env-}}\right). \tag{A18}$$

Now, assuming $\eta_{env+} \simeq \eta_{env-} \simeq 1$ according to Schrödinger's Zitterbewegung, T_{env} becomes, using Equation (A14):

$$T_{env} \simeq \frac{mc^2}{b_{env}}(N_{env-} + N_{env+}) \simeq \frac{1}{2}mc^2, \tag{A19}$$

and thus:

$$T_{nuc} = T - T_{env} \simeq \frac{1}{2}mc^2. \tag{A20}$$

The forthcoming study of the interactions between the nucleus and envelope will show that they are negligible compared to intra-component forces (nucleus onto itself, envelope onto itself). The two components therefore almost behave as two bound independent systems, and thus presumably obey the Virial theorem separately. Hence, since we have $T_{nuc} \simeq T_{env} \simeq mc^2/2$, we should also obtain $U_{nuc} \simeq U_{env} \simeq -mc^2$ so that the total energies amount to: $E_{nuc} \simeq E_{env} \simeq -mc^2/2$ and $E_{tot} \simeq -mc^2$.

Determination of η_{nuc}+ and η_{nuc}-

In order to determine η_{nuc^+} and η_{nuc^-}, considering Equations (A17) and (A20), we have:

$$\left(\frac{1}{\eta_{nuc+}} + \frac{1}{\eta_{nuc-}}\right) \simeq \frac{b_{nuc}}{2N_{nuc+}}. \tag{A21}$$

The latter expression, together with Equation (A4), can allow us to determine η_{nuc+} and η_{nuc-} in terms of N_{nuc+}, a_{anml}, n_{nuc}, and b_{nuc}:

$$\begin{aligned} &\frac{b_{nuc}}{2N_{nuc+}} \simeq \frac{1}{\eta_{nuc+}} + \frac{1}{\left(\eta_{nuc+} + \frac{a_{anml}n_{nuc}}{N_{nuc+}}\right)}, \\ &\frac{1}{\eta_{nuc+}}\left(\frac{b_{nuc}\eta_{nuc+}}{2N_{nuc+}} - 1\right) = \frac{1}{\eta_{nuc+}}\left(\frac{1}{1 + \frac{a_{anml}n_{nuc}}{N_{nuc+}\eta_{nuc+}}}\right), \\ &1 = \left(1 + \frac{a_{anml}n_{nuc}}{N_{nuc+}\eta_{nuc+}}\right)\left(\frac{b_{nuc}\eta_{nuc+}}{2N_{nuc+}} - 1\right), \\ &\eta_{nuc+}^2\left(\frac{b_{nuc}}{2N_{nuc+}}\right) + \eta_{nuc+}\left(\frac{a_{anml}b_{nuc}n_{nuc}}{2N_{nuc+}^2} - 2\right) \\ &\qquad - \left(\frac{a_{anml}n_{nuc}}{N_{nuc+}}\right) = 0, \\ &\Delta = 4 + \left(\frac{a_{anml}b_{nuc}n_{nuc}}{2N_{nuc+}^2}\right)^2, \end{aligned}$$

and taking the positive solution, we find:

$$\eta_{nuc+} = \frac{N_{nuc+}}{b_{nuc}}\left(2 - \frac{a_{anml}b_{nuc}n_{nuc}}{2N_{nuc+}^2} + \sqrt{4 + \left(\frac{a_{anml}b_{nuc}n_{nuc}}{2N_{nuc+}^2}\right)^2}\right), \tag{A22}$$

and η_{nuc-} can then be derived from Equation (A4).

Forces and Potentials

Centrifugal Force of a Triolet

Assuming triolets travel at light velocity, the centrifugal force [16] of triolet T_i, revolving along orbit of radius $\rho_i = \eta_i \lambda\!\!\!^{-}_C$, is in cylindrical coordinates:

$$F_{ctf,i} = \frac{p_i v_i}{\rho_i} = \frac{mc \cdot c}{b_i \eta_i \rho_i} = \frac{\hbar c}{b_i \rho_i^2}, \tag{B1}$$

where b_i stands for b_{env} (respectively, b_{nuc}) when T_i belongs to the envelope (resp. the nucleus). This expression applies both to nucleus and envelope triolets.

Electromagnetic Force Exerted on Nucleus Triolet *i* Due to Current at Envelope

The electromagnetic force exerted onto nucleus triolet i is given by the Lorentz force written using scalar potential V and vector potential $\mathbf{A}$:

$$\overrightarrow{\mathbf{F}}_{env\pm>i} = \frac{\mathrm{sgn}(i)\cdot e}{n_{nuc}}\left[-\overrightarrow{\nabla} V_{env\pm>i} - \frac{\partial}{\partial t}\overrightarrow{\mathbf{A}}_{env\pm>i} + c\hat{\theta} \times \left(\overrightarrow{\nabla} \times \overrightarrow{\mathbf{A}}_{env\pm>i}\right)\right], \tag{B2}$$

if all triolets revolve in the same positive direction. The expressions for the scalar and vector potentials and their derivatives must be determined.

As a net charge ($-e$) circulates around the envelope, the scalar potential and vector potential, for $r_{nuc} < r_{env}$ and $\cos\theta = 0$ (since the orbit is in the plane $z = 0$), are given [41] by:

$$V_{env\pm>i\in nuc} = \frac{Q_{env\pm}}{4\pi\varepsilon_0 r_{env\pm}} \sum_{l=0,2,4\ldots}^{\infty} [P_l(0)]^2 \left(\frac{\rho_i}{\rho_{env\pm}}\right)^l, \tag{B3}$$

$$A_{env\pm>i\in nuc} = \frac{\mu_0 I_{env\pm}}{2} \sum_{l=1,3,5\ldots}^{\infty} \frac{\left[P_l^1(0)\right]^2}{l(l+1)} \left(\frac{\rho_i}{\rho_{env\pm}}\right)^l, \tag{B4}$$

where the $P_l(x)$ and $P_l{}^1(x)$, respectively, designate the Legendre polynomials and associated Legendre polynomials, yielding:

$$V_{env\pm>i\in nuc} \simeq \frac{Q_{env\pm}}{4\pi\varepsilon_0}\left[\frac{1}{\rho_{env\pm}} + \frac{1}{4}\frac{\rho_i^2}{\rho_{env\pm}^3} + \frac{9}{64}\frac{\rho_i^4}{\rho_{env\pm}^5}\right], \tag{B5}$$

$$\frac{\partial V_{env\pm>i\in nuc}}{\partial \rho_{nuc\pm}} \simeq \frac{Q_{env\pm}}{4\pi\varepsilon_0}\left[\frac{1}{2}\frac{\rho_i}{\rho_{env\pm}^3} + \frac{9}{16}\frac{\rho_i^3}{\rho_{env\pm}^5}\right]. \tag{B6}$$

Recalling $\mu_0 = 1/(\varepsilon_0 c^2)$, $v = c$ and $Q_{env\pm} = \pm N_{env\pm} e / n_{env}$:

$$\frac{\mu_0 I_{env\pm}}{2} = \frac{\mu_0 Q_{env\pm}}{2t_{env\pm}} \simeq \frac{1}{2\varepsilon_0 c^2}\left(\frac{\pm N_{env\pm} e}{n_{env}}\right)\left(\frac{c}{2\pi\rho_{env\pm}}\right), \tag{B7}$$

$$A_{env\pm>i\in nuc} \simeq \frac{\pm N_{env\pm} e}{4\pi\varepsilon_0 c n_{env}}\left[\frac{1}{2}\frac{\rho_i}{\rho_{env\pm}^2} + \frac{3}{16}\frac{\rho_i^3}{\rho_{env\pm}^4}\right], \tag{B8}$$

$$\frac{\partial\left(A_{env\pm>i\in nuc}\hat{\boldsymbol{\theta}}\right)}{\partial t_{nuc}} = -A_{env\pm>i\in nuc}\frac{c}{\rho_{nuc}}\hat{\boldsymbol{\rho}} \simeq \frac{-(\pm N_{env\pm} e)}{4\pi\varepsilon_0 n_{env}}\left[\frac{1}{2\rho_{env\pm}^2} + \frac{3}{16}\frac{\rho_i^2}{\rho_{env\pm}^4}\right]\hat{\boldsymbol{\rho}}, \tag{B9}$$

$$\overrightarrow{\nabla} \times \overrightarrow{\mathbf{A}} = \begin{vmatrix} \hat{\boldsymbol{\rho}} & \hat{\boldsymbol{\theta}} & \hat{\mathbf{k}} \\ \frac{\partial}{\partial\rho} & \frac{\partial}{\rho\partial\theta} & \frac{\partial}{\partial z} \\ 0 & A_{env\pm>i\in nuc} & 0 \end{vmatrix} = \frac{\partial\left(A_{env\pm>i\in nuc}\right)}{\partial\rho_{nuc}}\hat{\boldsymbol{k}} \simeq \frac{(\pm N_{env\pm} e)}{4\pi\varepsilon_0 c n_{env}}\left[\frac{1}{2\rho_{env\pm}^2} + \frac{9}{16}\frac{\rho_i^2}{\rho_{env\pm}^4}\right]\hat{\mathbf{k}}. \tag{B10}$$

The electromagnetic force (B2) exerted on a nucleus triolet T_i by the envelope is then given by:

$$\overrightarrow{\mathbf{F}}_{env\pm>i\in nuc} \simeq \frac{-\mathrm{sgn}(i)}{n_{nuc}}\frac{\left(\pm N_{env\pm} e^2\right)}{4\pi\varepsilon_0 n_{env}\rho_{env\pm}^2}\left[\frac{1}{2}\frac{\rho_i}{\rho_{env\pm}} + \frac{3}{8}\frac{\rho_i^2}{\rho_{env\pm}^2} + \frac{9}{16}\frac{\rho_i^3}{\rho_{env\pm}^3}\right]\hat{\boldsymbol{\rho}}. \tag{B11}$$

Electromagnetic Force Exerted on Envelope Triolet *i* Due to Current Flowing at Nucleus

According to Equation (A3), the magnetic moment due to the nucleus is:

$$\mu_{nuc} = \frac{-a_{anml} e\hbar}{2m} = \frac{N_{nuc+} ec}{2n_{nuc}}\left(\rho_{nuc+} - \rho_{nuc-}\right). \tag{B12}$$

The vector potential and its derivatives are given [41] by:

$$\overrightarrow{\mathbf{A}}_{nuc>i\in env} \simeq \frac{\mu_0}{4\pi}\frac{\mu_{nuc}}{\rho_i^2}\hat{\boldsymbol{\theta}}, \tag{B13}$$

$$\overrightarrow{\mathbf{A}}_{nuc>i\in env} \simeq \frac{1}{8\pi\varepsilon_0 c}\frac{N_{nuc+} e}{n_{nuc}}\frac{\left(\rho_{nuc+} - \rho_{nuc-}\right)}{\rho_i^2}\hat{\boldsymbol{\theta}}, \tag{B14}$$

$$\frac{\partial\left(A_{nuc>i\in env}\hat{\boldsymbol{\theta}}\right)}{\partial t_i} = -A_{nuc>i\in env}\frac{c}{\rho_i}\hat{\boldsymbol{\rho}} = \frac{-1}{8\pi\varepsilon_0}\frac{N_{nuc+} e}{n_{nuc}}\frac{\left(\rho_{nuc+} - \rho_{nuc-}\right)}{\rho_i^3}\hat{\boldsymbol{\rho}} \tag{B15}$$

$$\overrightarrow{\nabla} \times \overrightarrow{\mathbf{A}} = \begin{vmatrix} \hat{\boldsymbol{\rho}} & \hat{\boldsymbol{\theta}} & \hat{\mathbf{k}} \\ \frac{\partial}{\partial\rho} & \frac{\partial}{\rho\partial\theta} & \frac{\partial}{\partial z} \\ 0 & A_{nuc>i\in env} & 0 \end{vmatrix} = \frac{\partial\left(A_{nuc>i\in env}\right)}{\partial\rho_i}\hat{\boldsymbol{k}} = \frac{(-1)}{4\pi\varepsilon_0 c}\frac{N_{nuc+} e}{n_{nuc}}\frac{\left(\rho_{nuc+} - \rho_{nuc-}\right)}{\rho_i^3}\hat{\mathbf{k}}. \tag{B16}$$

As the net nucleus charge is zero, and using Equation (A4), the force is defined by:

$$\overrightarrow{\mathbf{F}}_{nuc>i\in env} = \frac{\mathrm{sgn}(i)\cdot e}{n_{env}}\left[-\frac{\partial}{\partial t}\overrightarrow{\mathbf{A}}_{nuc>i} + c\hat{\theta}_j\left(\overrightarrow{\nabla} \times \overrightarrow{\mathbf{A}}_{nuc>i}\right)\right],$$

$$\overrightarrow{\mathbf{F}}_{nuc>i\in env} = \frac{3}{8\pi\varepsilon_0}\frac{\mathrm{sgn}(i)\, e^2 N_{nuc+}}{n_{nuc} n_{env}}\frac{\left(\eta_{nuc+} - \eta_{nuc-}\right)\lambda\!\!\!^{-}_C}{\rho_i^3}\hat{\boldsymbol{\rho}},$$

$$\overrightarrow{\mathbf{F}}_{nuc>i\in env} = \frac{-3}{8\pi\varepsilon_0}\frac{\mathrm{sgn}(i)\, e^2}{n_{env}}\frac{a_{anml}\lambda\!\!\!^{-}_C}{\rho_i^3}\hat{\boldsymbol{\rho}}. \tag{B17}$$

Electromagnetic Force Exerted on Triolet *i* at Radius ρ_i Due to Triolet *j* at Radius ρ_j

Every triolet experiences the fields emitted by all other triolets belonging to the same or adjacent orbit in the same component. Here we estimate the electromagnetic field and force exerted by a single triolet revolving on the same or adjacent orbit.

Let triolet T_j' ($\rho_j \sin\theta'_j$, $\rho_j \cos\theta'_j$) of charge q_j, revolving at light velocity on circular orbit of radius ρ_j, be positioned at angle θ'_j at retarded time t', and emitting an electromagnetic field received at time t by triolet $T_i(0, \rho_i)$ of charge q_i revolving at light velocity on circular orbit of radius ρ_i, and arriving at angle $\theta_i = 0$ on vertical axis y (**Figure 3A**). We have:

$$\overrightarrow{\mathbf{T_j T_i}} \begin{pmatrix} -\rho_j \ \sin\theta'_j \\ \rho_i - \rho_j \ \cos\theta'_j \end{pmatrix},$$

$$T_j T_i{}^2 = \rho_i^2 + \rho_j^2 - 2\rho_i\rho_j \cos\theta'_j \equiv R_{ij}^2, \tag{B18}$$

$$\hat{\mathbf{n}}_{ji} = \frac{\overrightarrow{\mathbf{T_j T_i}}}{T_j T_i} \begin{pmatrix} -\frac{\rho_j}{R_{ij}} \sin\theta'_j \\ \frac{\rho_i - \rho_j \ \cos\theta'_j}{R_{ij}} \end{pmatrix}, \tag{B19}$$

$$R_{ij} = \sqrt{\rho_i^2 + \rho_j^2 - 2\rho_i\rho_j \cos\theta'_j}. \tag{B20}$$

The trajectory, velocity and acceleration of triolet T_j are, respectively, given by:

$$\overrightarrow{\mathbf{w}}_j\left(t'\right) = \rho_j\left(\sin\omega t'\,\hat{\mathbf{x}} + \cos\omega t'\,\hat{\mathbf{y}}\right), \tag{B21}$$

$$\overrightarrow{\mathbf{v}}_j\left(t'\right) = \rho_j\omega\left(\cos\omega t'\,\hat{\mathbf{x}} - \sin\omega t'\,\hat{\mathbf{y}}\right), \tag{B22}$$

$$\overrightarrow{\mathbf{a}}_j\left(t'\right) = -\rho_j\omega^2\left(\sin\omega t'\,\hat{\mathbf{x}} + \cos\omega t'\,\hat{\mathbf{y}}\right), \tag{B23}$$

with ω being the angular velocity, satisfying relations $c = \rho\omega$ and $\theta' = \omega t'$. Since $v = c$, $\beta = v/c = 1$, we also have:

$$\hat{\boldsymbol{\rho}}_\mathbf{j}\begin{pmatrix}\sin\theta'_j\\ \cos\theta'_j\\ 0\end{pmatrix}, \quad \boldsymbol{\beta}_\mathbf{j}\begin{pmatrix}\cos\theta'_j\\ -\sin\theta'_j\\ 0\end{pmatrix}, \quad \dot{\boldsymbol{\beta}}_\mathbf{j}\begin{pmatrix}-c\sin\theta'_j/\rho_j\\ -c\cos\theta'_j/\rho_j\\ 0\end{pmatrix}$$

$$= \frac{-c}{\rho_j}\,\hat{\rho}_\mathbf{j}, \tag{B24}$$

$$g = 1 - \beta_\mathbf{j}\cdot\hat{\mathbf{n}}_{ji} = 1 - \cos\left(\frac{\pi}{2} + \gamma_j\right) = 1 + \sin\gamma_j. \tag{B25}$$

The electric and magnetic fields emitted by T_j and received by T_i are given [41] by:

$$\boldsymbol{E}_\mathbf{j} = \frac{q_j}{4\pi\varepsilon_0}\left[\frac{\left(\hat{\mathbf{n}}_{ji} - \boldsymbol{\beta}_\mathbf{j}\right)\left(1-\beta^2\right)}{g^3 R_{ij}^2} + \frac{\hat{\mathbf{n}}_{ji}\times\left[\left(\hat{\mathbf{n}}_{ji} - \boldsymbol{\beta}_\mathbf{j}\right)\times\dot{\boldsymbol{\beta}}_\mathbf{j}\right]}{cg^3 R_{ij}}\right] \tag{B26}$$

$$\boldsymbol{B}_\mathbf{j} = \frac{\mu_0 q_j}{4\pi}\left[\frac{\left(\mathbf{v_j}\times\hat{\mathbf{n}}_{ji}\right)\left(1-\beta^2\right)}{g^3 R_{ij}^2} + \frac{\left(\boldsymbol{\beta}_\mathbf{j}\times\hat{\mathbf{n}}_{ji}\right)\left(\dot{\boldsymbol{\beta}}_\mathbf{j}\cdot\hat{\mathbf{n}}_{ji}\right) + g\dot{\boldsymbol{\beta}}_\mathbf{j}\times\hat{\mathbf{n}}_{ji}}{g^3 R_{ij}}\right]. \tag{B27}$$

From **Figure 3B**, it can be seen that:

$$\dot{\boldsymbol{\beta}}_\mathbf{j}\cdot\hat{\mathbf{n}}_{ji} = \frac{c}{\rho_j}\cos\gamma_j, \tag{B28}$$

$$\cos\frac{\bar{\gamma}_j}{2} = \frac{1}{2}\left|\hat{\mathbf{n}}_{ji} - \boldsymbol{\beta}_\mathbf{j}\right|, \tag{B29}$$

$$\cos\frac{\bar{\gamma}_j}{2} = \sqrt{\frac{1}{2}\left(1+\cos\bar{\gamma}_j\right)} = \sqrt{\frac{1}{2}\left(1+\sin\gamma_j\right)}. \tag{B30}$$

And thus:

$$\hat{\mathbf{n}}_{ji}\cdot\left(\hat{\mathbf{n}}_{ji} - \boldsymbol{\beta}_\mathbf{j}\right) = \left|\hat{\mathbf{n}}_{ji} - \boldsymbol{\beta}_\mathbf{j}\right|\cdot\cos\frac{\gamma_j}{2} = 2\cos^2\frac{\gamma_j}{2} = 1 + \sin\gamma_j. \tag{B31}$$

From Equations (B25, B28) and identity: $\boldsymbol{a}\times(\boldsymbol{b}\times\boldsymbol{c}) = (\boldsymbol{a}\cdot\boldsymbol{c})\boldsymbol{b} - (\boldsymbol{a}\cdot\boldsymbol{b})\boldsymbol{c}$, we deduce:

$$\begin{aligned}\hat{\boldsymbol{n}}_{ji}\times\left[\left(\hat{\boldsymbol{n}}_{ji} - \boldsymbol{\beta}_\mathbf{j}\right)\times\dot{\boldsymbol{\beta}}_j\right] &= \left(\dot{\boldsymbol{\beta}}_j\cdot\hat{\boldsymbol{n}}_{ji}\right)\left(\hat{\boldsymbol{n}}_{ji} - \boldsymbol{\beta}_j\right) - \left[\hat{\boldsymbol{n}}_{ji}\cdot\left(\hat{\boldsymbol{n}}_{ji} - \boldsymbol{\beta}_j\right)\right]\dot{\boldsymbol{\beta}}_\mathbf{j},\\ \hat{\boldsymbol{n}}_{ji}\times\left[\left(\hat{\boldsymbol{n}}_{ji} - \boldsymbol{\beta}_\mathbf{j}\right)\times\dot{\boldsymbol{\beta}}_\mathbf{j}\right] &= \frac{c}{\rho_j}\cos\gamma_j\left(\hat{\boldsymbol{n}}_{ji} - \boldsymbol{\beta}_j\right) - \left(1+\sin\gamma_j\right)\dot{\boldsymbol{\beta}}_\mathbf{j},\end{aligned} \tag{B32}$$

implying, since $1-\beta^2 = 0$ and using Equations (B24, B25, B32):

$$\begin{aligned}\boldsymbol{E}_\mathbf{j} &= \frac{q_j}{4\pi\varepsilon_0}\left[\frac{\hat{\mathbf{n}}_{ji}\times\left[\left(\hat{\mathbf{n}}_{ji} - \boldsymbol{\beta}_j\right)\times\dot{\boldsymbol{\beta}}_j\right]}{cg^3 R_{ij}}\right],\\ \boldsymbol{E}_\mathbf{j} &= \frac{q_j}{4\pi\varepsilon_0 R_{ij}\rho_j}\left[\left(\hat{\mathbf{n}}_{ji} - \boldsymbol{\beta}_j\right)\frac{\cos\gamma_j}{\left(1+\sin\gamma_j\right)^3} + \hat{\boldsymbol{\rho}}_\mathbf{j}\frac{1}{\left(1+\sin\gamma_j\right)^2}\right].\end{aligned} \tag{B33}$$

From **Figure 3B**, we also have:

$$\boldsymbol{\beta}_j\times\hat{\mathbf{n}}_{ji} = -\sin\left(\frac{\pi}{2} + \gamma_j\right)\hat{\mathbf{z}} = -\cos\gamma_j\hat{\mathbf{z}}, \tag{B34}$$

$$\dot{\boldsymbol{\beta}}_j\times\hat{\mathbf{n}}_{ji} = -\frac{c\hat{\rho}_\mathbf{j}}{\rho_j}\times\hat{\mathbf{n}}_{ji} = -\frac{c}{\rho_j}\sin\left(\pi - \gamma_j\right)\hat{\mathbf{z}} = -\frac{c}{\rho_j}\sin\gamma_j\hat{\mathbf{z}}, \tag{B35}$$

yielding, using Equations (B27, B28) and $\mu_0 = 1/(\varepsilon_0 c^2)$:

$$\begin{aligned}\mathbf{B}_\mathbf{j} &= \frac{\mu_0 q_j}{4\pi}\left[\frac{-\frac{c}{\rho_j}\cos\gamma_j\cos\gamma_j - \frac{c}{\rho_j}(1+\sin\gamma_j)\sin\gamma_j}{(1+\sin\gamma_j)^3 R_{ij}}\right]\hat{\mathbf{z}},\\ \mathbf{B}_\mathbf{j} &= \frac{-q_j}{4\pi\varepsilon_0 c R_{ij}\rho_j\left(1+\sin\gamma_j\right)^2}\hat{\mathbf{z}}.\end{aligned} \tag{B36}$$

The magnetic force is directed along $\boldsymbol{\rho_i}$ since $\boldsymbol{B}_j$ is along $\boldsymbol{z}$. But to express the equilibrium we need to find the component of $\boldsymbol{E_j}$ along $\boldsymbol{\rho_i}$, and thus we need:

$$\hat{\mathbf{n}}_{ji}\cdot\hat{\boldsymbol{\rho}}_\mathbf{i} = \frac{1}{R_{ij}}\left(\rho_i - \rho_j\ \cos\theta'_j\right), \tag{B37}$$

$$\hat{\boldsymbol{\rho}}_\mathbf{i}\cdot\left(-\boldsymbol{\beta}_\mathbf{j}\right) = \cos\left(\theta'_j - \frac{\pi}{2}\right) = \sin\theta'_j, \tag{B38}$$

$$\hat{\boldsymbol{\rho}}_\mathbf{i}\cdot\hat{\boldsymbol{\rho}}_\mathbf{j} = \cos\theta'_j, \tag{B39}$$

yielding from Equation (B33):

$$\boldsymbol{E}_{\mathbf{ji}\perp} = \frac{q_j}{4\pi\varepsilon_0 R_{ij}\rho_j}\left[\frac{1}{R_{ij}}\left(\rho_i - \rho_j\ \cos\theta'_j\right)\frac{\cos\gamma_j}{\left(1+\sin\gamma_j\right)^3}\right.$$

$$+\frac{\sin\theta_j^{'}\cos\gamma_j}{\left(1+\sin\gamma_j\right)^3}+\frac{\cos\theta_j^{'}}{\left(1+\sin\gamma_j\right)^2}\Bigg]\hat{\boldsymbol{\rho}}. \quad \text{(B40)}$$

This can be rearranged by expressing θ'_j as a function of γ_j and vice versa. From Equations (B19, B24):

$$\begin{aligned}\cos\gamma_j &= -\hat{\boldsymbol{\rho}}_{\mathbf{j}}\cdot\hat{\mathbf{n}}_{ji} = -\sin\theta_j^{'}\left(-\frac{\rho_j}{R_{ij}}\sin\theta_j^{'}\right)\\ &\quad -\cos\theta_j^{'}\left(\frac{\rho_i-\rho_j\cos\theta_j^{'}}{R_{ij}}\right),\\ \cos\gamma_j &= \frac{1}{R_{ij}}\left(\rho_j-\rho_i\cos\theta_j^{'}\right). \quad \text{(B41)}\end{aligned}$$

Similarly, from Equation (B28):

$$\begin{aligned}\sin\gamma_j\,\hat{\mathbf{z}} &= \hat{\boldsymbol{\rho}}_{\mathbf{j}}\times\hat{\mathbf{n}}_{ji} = \begin{vmatrix}\hat{\boldsymbol{x}} & \hat{\boldsymbol{y}} & \hat{\boldsymbol{z}}\\ \sin\theta_j^{'} & \cos\theta_j^{'} & 0\\ -\frac{\rho_j}{R_{ij}}\sin\theta_j^{'} & \frac{\rho_i-\rho_j\cos\theta_j^{'}}{R_{ij}} & 0\end{vmatrix},\\ \sin\gamma_j &= \frac{\rho_i}{R_{ij}}\sin\theta_j^{'}. \quad \text{(B42)}\end{aligned}$$

Relations (B41) and (B42) may be reversed:

$$\begin{aligned}\sin\theta_j^{'} &= \frac{R_{ij}}{\rho_i}\sin\gamma_j, \quad \text{(B43)}\\ \cos\theta_j^{'} &= \frac{1}{\rho_i}\left(\rho_j-R_{ij}\cos\gamma_j\right). \quad \text{(B44)}\end{aligned}$$

Then, using these to rearrange Equation (B40) and developing:

$$\begin{aligned}&\frac{1}{R_{ij}^2}\left(\rho_i-\rho_j\cos\theta_j^{'}\right)\left(\rho_j-\rho_i\cos\theta_j^{'}\right)\\ &\quad=\frac{1}{R_{ij}^2}\left[\rho_i\rho_j\sin^2\theta_j^{'}-R_{ij}^2\cos\theta_j^{'}\right],\\ &\frac{\sin\theta_j^{'}}{R_{ij}}\left(\rho_j-\rho_i\cos\theta_j^{'}\right)+\cos\theta_j^{'}\left(1+\frac{\rho_i}{R_{ij}}\sin\theta_j^{'}\right)\\ &\quad=\cos\theta_j^{'}+\frac{\rho_j}{R_{ij}}\sin\theta_j^{'},\end{aligned}$$

we obtain using Equation (B42):

$$\begin{aligned}\boldsymbol{F}_{\mathbf{ji}\perp} &= \frac{q_j\sin\theta_j^{'}}{4\pi\varepsilon_0 R_{ij}^2\left(1+\sin\gamma_j\right)^3}\left[\frac{\rho_i}{R_{ij}}\sin\theta_j^{'}+1\right]\hat{\boldsymbol{\rho}},\\ \boldsymbol{F}_{\mathbf{ji}\perp} &= \frac{q_j\sin\gamma_j}{4\pi\varepsilon_0 R_{ij}\rho_i\left(1+\sin\gamma_j\right)^2}\hat{\boldsymbol{\rho}}. \quad \text{(B45)}\end{aligned}$$

The Lorentz force is then:

$$\begin{aligned}\boldsymbol{F}_{\mathbf{ij}\perp} &= q_i\left(\boldsymbol{E}_{\mathbf{ij}\perp}+c\hat{\theta}_i\times\boldsymbol{B}_{\mathbf{ij}}\right),\\ \boldsymbol{F}_{\mathbf{ij}\perp} &= \frac{q_iq_j}{4\pi\varepsilon_0 R_{ij}\rho_i}\left[\frac{\sin\gamma_j}{\left(1+\sin\gamma_j\right)^2}\right]\hat{\boldsymbol{\rho}}\\ &\quad+\frac{q_iq_j}{4\pi\varepsilon_0 R_{ij}\rho_j}\left[\frac{1}{\left(1+\sin\gamma_j\right)^2}\right]\hat{\boldsymbol{\rho}},\\ \boldsymbol{F}_{\mathbf{ij}\perp} &= \frac{q_iq_j}{4\pi\varepsilon_0 R_{ij}\left(1+\sin\gamma_j\right)^2}\left[\frac{\sin\gamma_j}{\rho_i}+\frac{1}{\rho_j}\right]\hat{\boldsymbol{\rho}}. \quad \text{(B46)}\end{aligned}$$

The scalar and vector Liénard-Wichert retarded electromagnetic potentials [41] are:

$$\begin{aligned}V_{ij} &= \frac{q_j}{4\pi\varepsilon_0\left(R_{ij}-\boldsymbol{\beta}_{\mathbf{j}}\cdot\mathbf{R}_{\mathbf{ij}}\right)_{rtrd}} = \frac{q_j}{4\pi\varepsilon_0 R_{ij}\left(1+\sin\gamma_j\right)}, \quad \text{(B47)}\\ \boldsymbol{A}_{\mathbf{ij}} &= \frac{\mu_0}{4\pi}\left(\frac{q_jv_j\hat{\theta}_j}{R_{ij}-\boldsymbol{\beta}_{\mathbf{j}}\cdot\mathbf{R}_{\mathbf{ij}}}\right)_{rtrd} = \frac{q_j\hat{\theta}_j}{4\pi\varepsilon_0 cR_{ij}\left(1+\sin\gamma_j\right)}. \quad \text{(B48)}\end{aligned}$$

Approximation ρ_i=ρ_j. When making this approximation (one-orbit model), from **Figure 3C**, R_{ij} becomes:

$$R_{ij}=2\rho_i\cos\gamma_j. \quad \text{(B49)}$$

Note that if ρ_i= ρ_j, Equation (B46) then becomes:

$$\mathbf{F}_{\mathbf{ij}\perp}=\frac{q_iq_j}{8\pi\varepsilon_0\rho_i^2\cos\gamma_j\left(1+\sin\gamma_j\right)}\hat{\boldsymbol{\rho}}. \quad \text{(B50)}$$

Triolets at Radial Equilibrium

Equilibrium of Envelope Triolets

Envelope triolets are submitted to the centrifugal force (B1), the magnetic force due to the net nucleus magnetic moment (B17), and the net electromagnetic force due to the other envelope triolets (B46). Equilibrium for env– triolets can be written:

$$\begin{aligned}0 &= \frac{\hbar c}{b_{env}\rho_{env-}^2}+\frac{(-e)}{n_{env}}\sum_j^{N_{env}-1}\frac{e}{n_{env}}\frac{1}{4\pi\varepsilon_0}\frac{\mathrm{sgn}\left(j\right)}{R_{ij}(1+\sin\gamma_j)^2}\\ &\quad\times\left[\frac{\sin\gamma}{\rho_{env-}}+\frac{1}{\rho_j}\right]+\frac{3}{8\pi\varepsilon_0}\frac{e^2}{n_{env}}\frac{a_{anml}\lambda\!\!\!^{-}_C}{\rho_{env-}^3}.\end{aligned}$$

And rearranging to isolate the fine-structure constant:

$$\begin{aligned}\frac{4\pi\varepsilon_0\hbar c}{e^2} &= \frac{1}{\alpha} = \frac{b_{env}\rho_{env-}^2}{n_{env}}\left[\sum_j^{N_{env}-1}\frac{1}{n_{env}}\frac{\mathrm{sgn}\left(j\right)}{R_{ij}(1+\sin\gamma_j)^2}\right.\\ &\quad\left.\times\left(\frac{\sin\gamma}{\rho_{env-}}+\frac{1}{\rho_j}\right)-\frac{3a_{anml}\lambda\!\!\!^{-}_C}{2\rho_{env-}^3}\right]. \quad \text{(C1)}\end{aligned}$$

Likewise, equilibrium for env+ triolets can be written:

$$\begin{aligned}\frac{1}{\alpha} &= \frac{b_{env}\rho_{env+}^2}{n_{env}}\left[-\sum_j^{N_{env}-1}\frac{1}{n_{env}}\frac{\mathrm{sgn}\left(j\right)}{R_{ij}(1+\sin\gamma_j)^2}\left(\frac{\sin\gamma}{\rho_{env+}}+\frac{1}{\rho_j}\right)\right.\\ &\quad\left.+\frac{3a_{anml}\lambda\!\!\!^{-}_C}{2\rho_{env+}^3}\right]. \quad \text{(C2)}\end{aligned}$$

Neglecting the term due to the nucleus magnetic moment, the equations become:

$$\frac{1}{\alpha} = \frac{-b_{env}}{n_{env}^2}\left[\sum_{j}^{N_{env}-1}\frac{\rho_i^2 \mathrm{sgn}\left(i\cdot j\right)}{R_{ij}(1+\sin\gamma_j)^2}\left(\frac{\sin\gamma}{\rho_i}+\frac{1}{\rho_j}\right)\right] \equiv G_{env}. \quad \text{(C3)}$$

The fine structure constant therefore appears to be naturally related to the ratio between the centrifugal force and the net electromagnetic force experienced by a single triolet. Making the ρ_i=ρ_j approximation (B49), we obtain:

$$\frac{1}{\alpha} = \frac{-b_{env}}{2n_{env}^2}\left[\sum_{j}^{N_{env}-1}\frac{\mathrm{sgn}\left(i\cdot j\right)}{\cos\gamma_j(1+\sin\gamma_j)}\right]. \quad \text{(C4)}$$

Equilibrium of Nucleus Triolets

Nucleus triolets are submitted to the centrifugal force (B1), the electromagnetic force due to the envelope (B11), and the net electromagnetic force due to the other nucleus triolets (B46). Equilibrium for nuc– triolets is thus written:

$$\frac{1}{\alpha} \simeq \frac{b\rho_{nuc-}^2}{n_{nuc}}\left[\frac{\rho_{nuc-}}{2n_{env}}\left(\frac{N_{env+}}{\rho_{env+}^3}-\frac{N_{env-}}{\rho_{env-}^3}\right) + \sum_{j}^{N_{nuc}-1}\frac{1}{n_{nuc}}\frac{\mathrm{sgn}\left(j\right)}{R_{ij}\left(1+\sin\gamma_j\right)^2}\left(\frac{\sin\gamma}{\rho_{nuc-}}+\frac{1}{\rho_j}\right)\right]. \quad \text{(C5)}$$

Similarly we have for the nuc+ triolets:

$$\frac{1}{\alpha} \simeq \frac{b\rho_{nuc+}^2}{n_{nuc}}\left[\frac{\rho_{nuc+}}{2n_{env}}\left(\frac{N_{env+}}{\rho_{env+}^3}-\frac{N_{env-}}{\rho_{env-}^3}\right) - \sum_{j}^{N_{nuc}-1}\frac{1}{n_{nuc}}\frac{\mathrm{sgn}\left(j\right)}{R_{ij}\left(1+\sin\gamma_j\right)^2}\left(\frac{\sin\gamma}{\rho_{nuc+}}+\frac{1}{\rho_j}\right)\right]. \quad \text{(C6)}$$

Neglecting the term due to the envelope current, the equations become:

$$\frac{1}{\alpha} = \frac{-b_{nuc}}{n_{nuc}^2}\left[\sum_{j}^{N_{nuc}-1}\frac{\rho_i^2 \mathrm{sgn}\left(i\cdot j\right)}{R_{ij}(1+\sin\gamma_j)^2}\left(\frac{\sin\gamma}{\rho_i}+\frac{1}{\rho_j}\right)\right] \equiv G_{nuc}. \quad \text{(C7)}$$

Making the ρ_i=ρ_j approximation (B49), we obtain:

$$\frac{1}{\alpha} = \frac{-b_{nuc}}{2n_{nuc}^2}\left[\sum_{j}^{N_{nuc}-1}\frac{\mathrm{sgn}\left(i\cdot j\right)}{\cos\gamma_j(1+\sin\gamma_j)}\right]. \quad \text{(C8)}$$

Also, the correction due to envelope current (first two terms) is:

$$G_{env>i\in nuc} \approx \frac{-b_{nuc}\mathrm{sgn}\left(i\right)\left(-n_{env}\right)}{n_{nuc}n_{env}}\left[\frac{\rho_{nuc}^3}{2\rho_{env}^3}+\frac{3\rho_{nuc}^4}{8\rho_{env}^4}\right] \approx \frac{b_{nuc}\mathrm{sgn}\left(i\right)}{n_{nuc}}\left[\frac{\eta_{nuc}^3}{2}+\frac{3\eta_{nuc}^4}{8}\right]. \quad \text{(C9)}$$

Retarted Angles

Evaluating the Values of Retarded Angle θ_j' From Non-retarded Angle θ_j

If we suppose triolets are uniformly distributed along the circular orbits (this is certainly true of the nucleus since we have N_{nuc+} = N_{nuc-}, but is an approximation in the case of the envelope, as there are more negative than positive triolets), then angle θ_j (expressed in radians) determining the position of the j^{th} triolet (starting at 1) at non-retarded time t on the orbit is defined by:

$$\theta_{j\in nuc} = 2\pi\frac{j}{N_{nuc}}. \quad \text{(D1)}$$

Note that, for the envelope, we also need to account for the empty space of length d_{env} (using the number of missing triolets as units) separating the n_{env} stretches of triolets, yielding for triolets T_j belonging to the first stretch:

$$\theta_{j\in 1stStretch} = 2\pi\frac{j}{\left(N_{env}+n_{env}d_{env}\right)}. \quad \text{(D2)}$$

To evaluate θ_j' determining the angular position T_j' at retarded time t' when the electromagnetic field was emitted toward triolet T_i, which arrives at angle 0 (vertical y axis) at time t to receive the field, we use the following relation, derived from **Figure 3A**:

$$R_{ij} = \rho_j\delta\theta_j = \rho_j\left(\theta_j-\theta_j^{'}\right). \quad \text{(D3)}$$

Then squaring Equations (B20) and (D3) and equating, we obtain:

$$\left(\theta_j-\theta^{'}{}_j\right)^2 = 1-2\left(\frac{\rho_i}{\rho_j}\right)\cos\theta^{'}{}_j+\left(\frac{\rho_i}{\rho_j}\right)^2. \quad \text{(D4)}$$

Given ρ_i, ρ_j, and θ_j, the retarded angles θ'$_j$ may be numerically determined by recurrence, using a computer program that implements Newton method for instance, to resolve transcendental Equation (D4) for all triolets of angular position θ_j expressed in radians. The corresponding values of γ_j are then estimated using Equation (B42).

Potential Energy

Electric Potential Energy

By definition, the electric potential energies at the envelope and nucleus are defined by:

$$U_{elec,env} = \sum_{i}^{N_{env}}\sum_{j\neq i}^{N_{env}-1} q_iV_{ij} = \sum_{i\in env}\sum_{j\neq i}\frac{q_iq_j}{4\pi\varepsilon_0R_{ij}\left(1+\sin\gamma_j\right)}, \quad \text{(E1)}$$

$$U_{elec,env} = \frac{\alpha mc^2}{n_{env}^2}\sum_{i\in env}\sum_{j\neq i}\frac{\mathrm{sgn}(i\cdot j)}{H_{ij}\left(1+\sin\gamma_j\right)}, \quad \text{(E2)}$$

where $H_{ij} = R_{ij}/\lambda\!\!\!^{-}_c$. Likewise, we have:

$$U_{elec,nuc} = \frac{\alpha mc^2}{n_{nuc}^2}\sum_{i\in nuc}\sum_{j\neq i}\frac{\mathrm{sgn}(i\cdot j)}{H_{ij}\left(1+\sin\gamma_j\right)}. \quad \text{(E3)}$$

Making the $\rho_i = \rho_j$ approximation (B49), we obtain:

$$U_{elec,env} = \frac{\alpha mc^2}{2n_{env}^2} \sum_{i\in env} \sum_{j\neq i} \frac{\mathrm{sgn}(i\cdot j)}{\eta_j \cos\gamma_j \left(1+\sin\gamma_j\right)}, \quad \text{(E4)}$$

$$U_{elec,nuc} = \frac{\alpha mc^2}{2n_{nuc}^2} \sum_{i\in nuc} \sum_{j\neq i} \frac{\mathrm{sgn}(i\cdot j)}{\eta_j \cos\gamma_j \left(1+\sin\gamma_j\right)}. \quad \text{(E5)}$$

Magnetic Potential Energy

The magnetic potential energy U_{mag} and electric potential energy U_{elec} are, respectively, the opposite of the magnetic work and electric work [41] given by:

$$W_{mag} = \frac{1}{2\mu_0} \int_{all\ space} B^2 d\tau = -U_{mag}, \quad \text{(E6)}$$

$$W_{elec} = \frac{\varepsilon_0}{2} \int_{all\ space} E^2 d\tau = -U_{elec}. \quad \text{(E7)}$$

Now, the vector expression relating the magnetic field to the electric field:

$$\overrightarrow{\boldsymbol{B}} = \frac{1}{c}\hat{\boldsymbol{n}} \times \overrightarrow{\boldsymbol{E}} \quad \text{(E8)}$$

holds in relativistic electrodynamics with particles going at light velocity, yielding:

$$W_{mag} = \frac{1}{2\mu_0 c^2} \int_{all\ space} E^2 d\tau, \quad \text{(E9)}$$

and since we know that $c^2 = 1/\varepsilon_0\mu_0$, we have:

$$W_{mag} = \frac{\varepsilon_0}{2} \int_{all\ space} E^2 d\tau = W_{elec}. \quad \text{(E10)}$$

Therefore:

$$U_{mag} = U_{elec}. \quad \text{(E11)}$$

Total Potential Energy

Neglecting the potential energy of the envelope acting on the nucleus $U_{env>nuc}$, and the potential energy of the nucleus acting on the envelope $U_{nuc>env}$, the electron potential energy is approximately:

$$U_{tot} \simeq U_{env} + U_{nuc}, \quad \text{(E12)}$$

where U_{env} is the envelope potential energy and U_{nuc} the nucleus potential energy. Using Equations (E2, E11), we obtain:

$$U_{env} = U_{env,mag} + U_{env,elec} = 2U_{env,elec}, \quad \text{(E13)}$$

$$U_{env} = \frac{2\alpha mc^2}{n_{env}^2} \sum_{i\in env} \sum_{j\neq i} \frac{\mathrm{sgn}(i\cdot j)}{H_{ij}\left(1+\sin\gamma_j\right)}, \quad \text{(E14)}$$

where $H_{ij} = R_{ij}/\lambda\!\!\!^{-}_{c}$. Likewise, using Equation (E.3) we have:

$$U_{nuc} = \frac{2\alpha mc^2}{n_{nuc}^2} \sum_{i\in nuc} \sum_{j\neq i} \frac{\mathrm{sgn}(i\cdot j)}{H_{ij}\left(1+\sin\gamma_j\right)}. \quad \text{(E15)}$$

Compatibility Between Potential Energies and Radial Equilibrium Equations

It can be shown that Equations (E14, E15) are compatible with Equations (C4, C8) if we assume $\eta_{nuc+} \simeq \eta_{nuc-}$ and $\eta_{env+} \simeq \eta_{env-} \simeq 1$. Indeed, Equation (C4) becomes:

$$\left[\sum_{j}^{N_{env}-1} \frac{\mathrm{sgn}\left(i\cdot j\right)}{2\cos\gamma_j(1+\sin\gamma_j)}\right] \simeq \frac{-n_{env}^2}{\alpha b_{env}}.$$

Then, by replacing the relation above into Equation (98), since $\eta_{env+} \simeq \eta_{env-} \simeq 1$, we obtain:

$$U_{env} = \frac{2\alpha mc^2}{n_{env}^2} \sum_{i\in env} \sum_{j\neq i} \frac{\mathrm{sgn}\left(i\cdot j\right)}{2\eta_i \cos\gamma_j \left(1+\sin\gamma_j\right)}$$

$$\simeq \frac{-2\alpha mc^2}{n_{env}^2} N_{env} \frac{n_{env}^2}{\alpha b_{env}},$$

$$U_{env} \simeq \frac{-2N_{env}mc^2}{b_{env}}.$$

Since $b_{env} = 2N_{env}$, this yields: $U_{env} \simeq -mc^2$ as expected. Likewise, Equation (C8) becomes:

$$\left[\sum_{j}^{N_{nuc}-1} \frac{\mathrm{sgn}\left(i\cdot j\right)}{2\cos\gamma_j(1+\sin\gamma_j)}\right] \simeq \frac{-n_{nuc}^2}{\alpha b_{nuc}}.$$

Then, by replacing the relation above into Equation (E15), we obtain:

$$U_{nuc} = \frac{2\alpha mc^2}{n_{nuc}^2} \sum_{i\in nuc} \sum_{j\neq i} \frac{\mathrm{sgn}(i\cdot j)}{2\eta_i \cos\gamma_j \left(1+\sin\gamma_j\right)} \simeq \frac{-2\alpha mc^2}{n_{nuc}^2} \frac{N_{nuc}}{\eta_{nuc}} \frac{n_{nuc}^2}{\alpha b_{nuc}},$$

$$U_{nuc} \simeq \frac{-2N_{nuc}mc^2}{b_{nuc}\eta_{nuc}}.$$

Since $2N_{nuc} = b_{nuc}\eta_{nuc}$ (A21), we obtain: $U_{nuc} \simeq -mc^2$ as expected.

Optimization Algorithm

An optimization algorithm has been devised and implemented to determine a set of optimum orbital radii for envelope triolets by minimizing average absolute deviation K, in the n-orbits model where each triolet possesses a specific radii η_i at the envelope. An approximate solution is determined heuristically before applying this algorithm. The algorithm next considers in turn every envelope triolet belonging to the first stretch, tries five different radii surrounding the current radius, and computes for each the stability of all envelope triolets. The radius yielding best overall stability is then attributed to the corresponding triolets in all six stretches. Once the procedure has been applied to all triolets of the first stretch, it is run again, considering five closer radii this time (thus slowly reducing the noise), until convergence toward an optimum solution is reached. The corresponding pseudocode is shown below. The algorithm was applied with the following values: delta = 0.00201, step = 0.00005, n_{env}= 6, N_{env+} = 60, N_{env-} = 66, $d_{env} = 2$.

```
Function optimize_env_radii( radius[126], delta, step ):
    for d in range( delta to 0.00001 by –step ):
        for i in range( 0 to 20 by +1 ):
            previous_radius = radius[ i ]
            R = previous_radius
            best_r = R
            best_K = 10000
            list_new_radii = { R−2d, R–d, R, R+d, R+2d }
            for r in list_new_radii:
                set_radius( i to r in all six stretches )
                clear( list_inv_alphas )
                for j in range( 1 to 20 by +1 ):
                    G = compute_inv_alpha( i, j )
                    add( G to list_inv_alphas )
                K = compute_error_K( list_inv_alphas )
                if K < best_K:
                    best_K = K
                    best_r = r
            set_radius( i to best_r in all six stretches )
return radius[126]
```

DATA AVAILABILITY STATEMENT

All datasets generated for this study are included in the article/supplementary material.

AUTHOR CONTRIBUTIONS

SA conceived the study, formed the hypotheses, constructed the model, wrote down and solved the equations, implemented the computations, and wrote the manuscript. FB helped solve the equations, devised the optimization algorithm, independently implemented the computations, and reviewed the manuscript. All authors approved the submitted version.

ACKNOWLEDGMENTS

The authors wish to thank Patrick Richard (IFSTTAR, University Gustave Eiffel) for helpful advice and Gilles Salbert (IGDR, University of Rennes 1) for support and reading the manuscript.

REFERENCES

1. Bourilkov D. Hint for axial-vector contact interactions in the data on $e^+e^- \rightarrow e^+e^-(\gamma)$ at center-of-mass energies 192-208 GeV. *Phys Rev* D. (2001) **64:**071701. doi: 10.1103/PhysRevD.64.071701
2. Davisson CJ, Germer LH. Diffractions of electrons by a crystal of Nickel. *Phys. Rev*. (1927) **30**:705.
3. Bohr N. The quantum postulate and the recent development of atomic theory. *Nature*. (1928) **121:**580–90.
4. Heisenberg W. Das naturgesetz und die struktur der materie, belser-presse, 1967. trans. *Natural Law and The Structure of Matter*. Belser: Warm Wind Books (1981).
5. de Broglie L. Treize remarques sur divers sujets de physique théorique. *Ann. Fond. L. de Broglie*. (1976) **1**:116–28.
6. Dirac P. An extensible model of the electron. *Proc. Royal Soc. Lond A*. (1962) **268**:57–67.
7. Bunge M. A picture of the electron. *Nuovo Cimento*. (1955) **1**:977–85.
8. Abraham M. Prinzipien der dynamik des elektrons. *Ann Phys*. (1903) **1**:105–79.
9. Lorentz HA. *The Theory of Electrons*. 2nd ed. Leipzig: Teubner (1916).
10. Fermi E. Über einen Widerspruch zwischen der elektrodynamischen und relativistischen theorie der elektromagnetischen masse. *Phys Zeitschrift*. (1922) **23:**341–4.
11. Dirac P. Classical theory of radiating electrons. *Proc Royal Soc Lond A*. (1938) **167**:148.
12. Rohrlich F. Self-energy and stability of the classical electron. *Am J Phys*. (1960) **28:**639.
13. Schwinger J. Electromagnetic mass revisited. *Found Phys*. (1983) **13**:373–83.
14. Parson AL. A magneton theory of the structure of the atom smithson. *Misc Collect*. (1915) **65**:1–80.
15. Webster LW. The theory of electromagnetic mass of the parson magneton and other non-spherical systems. *Phys Rev*. (1917) **9**:484–99.
16. Allen HS. The case for a ring electron. *Proc Phys Soc Lond*. (1918) **31**:49.
17. Compton AH. The size and shape of the electron. *Phys Rev*. (1919) **14**:247.
18. Poincaré H. Sur la dynamique de l'électron. *Rend Circolo Mat Palermo*. (1906) **21**:129–76.
19. Eisberg R, Resnick R. *Quantum Physics of Atoms, Molecules, Solids, Nuclei and Particles*, 2nd ed. Hamilton, ON: John Wiley and Sons (1985).
20. Griffiths DJ. *Introduction to Elementary Particles*, 2nd ed. Weinheim: Wiley-VCH. (2008). doi: 10.1002/9783527618460. index
21. Born M. Quantenmechanik der Stoßvorgänge. *Zeitschrift für Physik*. (1926) **38:**803–27.
22. Schrödinger E. Uber die kraftefreie Bewegung in der relativistischen Quantum-mechanik, Sitz. *Preuss. Akad. Wiss. Physik-Math*. (1930) **24**:418.
23. de Broglie L. La mécanique ondulatoire et la structure atomique de la matière et du rayonnement. *J Phys Radium*. (1927) **8**:225–41.
24. Bohm D. A suggested interpretation of the quantum theory in terms of hidden variables. *Phys Rev*. (1952) **85**:166. doi: 10.1103/PhysRev.85.166
25. Bohm D, Vigier JP. Model of the causal interpretation of quantum theory in terms of a fluid with irregular fluctuations. *Phys Rev*. (1954) **96**:208–16.
26. Bohm D, Dewdney C, Hiley BH. A quantum approach to the Wheeler delayed-choice experiment. *Nature*. (1985) **315**:294–7.
27. Weyssenhoff J. On two relativistic models of dirac's electron. *Acta Phys Pol*. (1947) **9**:47–53.
28. Huang K. On the zitterbewegung of the dirac electron. *Am J Phys*. (1952) **20**:479–84.
29. Barut AO, Bracken AJ. Zitterbewegung and the internal geometry of the electron. *Phys Rev D*. (1981) **23**:10.
30. Barut AO, Zanghi N. Classical model of the dirac electron. *Phys Rev Lett*. (1984) **52**:2009.
31. Bergman DL, Wesley JP. Spinning charge ring model of electron yielding anomalous magnetic moment. *Galilean Electrodynamics*. (1990) **1**:63–7.
32. Pavšič M, Recami E, Rodrigues WA Jr, Maccarrone GD, Raciti F, Salesi G. Spin and electron structure. *Phys Lett B*. (1993) **318**:481–8.
33. Salesi G, Recami E. Hydrodynamical reformulation and quantum limit of the barut-zanghi theory, found. *Phys Lett*. (1997) **10**:533–46.
34. Barut AO, Pavšič M. Radiation reaction and the electromagnetic energy-momentum of moving relativistic charged membranes. *Phys Lett B*. (1994) **331**:45–50.
35. Bostick WH. Mass, charge and current: the essence and morphology. *Physics Essays*. (1991) **4**:45.
36. Consa O. Helical solenoid model of the electron. *Progr Phys*. (2018) **14**:80–89.
37. Hestenes D. Quantum mechanics from self-interaction. *Found Phys*. (1985) **15**:63–87.
38. Hestenes D. The zitterbewegung interpretation of quantum mechanics. *Found Phys*. (1990) **20**:1213–32.
39. Odom B, Hanneke D, D'Urso B, Gabrielse G. New measurement of the electron magnetic moment using a one-electron quantum cyclotron. *Phys Rev Lett*. (2006) **97**:030801.

40. Goldstein H, Poole C, Safko J. *Classical Mechanics*, 3rd ed. Longman: Addison Wesley (2002). doi: 10.1119/1.1484149
41. Zangwill A. *Modern Electrodynamics*. Cambridge: Cambridge University Press (2013).
42. Pusey MF, Barrett J, Rudolph T. On the reality of the quantum state. *Nat Phys*. (2012) **8**:475–8.
43. Bell JS. On the impossible pilot wave. *Found Phys*. (1982) **12**:989–99.
44. von Neumann J. *Mathematical Foundations of Quantum Mechanics*. Princeton, NJ: Princeton Univ. Press (1955).
45. Wheeler JA, Zurek WH. *Quantum Theory and Measurement*. Princeton, NJ: Princeton University Press (1983).
46. Einstein A. Physics and reality. *J Franklin Institute*. (1936) **221**:349–82.
47. Dürr D, Goldstein S, Zanghi N. Quantum equilibrium and the origin of absolute uncertainty. *J Stat Phys*. (1992) **67**:843–907. doi: 10.1007/BF01049004
48. Hudson JJ, Kara DM, Smallman IJ, Sauer BE, Tarbutt MR, Hinds EA. Improved measurement of the shape of the electron. *Nature*. (2011) **473:**493–6. doi: 10.1038/nature10104
49. Kim BJ, Koh H, Rotenberg E, Oh SJ, Eisaki H, Motoyama N, et al. Distinct spinon and holon dispersions in photoemission spectral functions from one-dimensional $SrCuO_2$. *Nat Phys*. (2006) **2**:397–401. doi: 10.1038/nphys316
50. Jompol Y, Ford CJB, Griffiths JP, Farrer I, Jones GAC, Anderson D, et al. Probing spin-charge separation in a tomonaga-luttinger liquid. *Science*. (2009) **325**:597–601. doi: 10.1126/science.1171769
51. Schlappa J, Wohlfeld K, Zhou KJ, Mourigal M, Haverkort MW, Strocov VN, et al. Spin-orbital separation in the quasi-one-dimensional Mott insulator Sr_2CuO_3. *Nature*. (2012) **485**:82–5. doi: 10.1038/nature10974
52. Eidelman S, Hayes KG, Olive KA, Aguilar-Benitez M, Amsler C, Asner D. (Particle Data Group). Review of particle physics. *Phys Lett B*. (2004) **592**:1–5.

Conflict of Interest: The authors declare that the research was conducted in the absence of any commercial or financial relationships that could be construed as a potential conflict of interest.